# Initial assessment of all-season Arctic sea ice thickness from ICESat-2

Alek PETTY[1], Alex CABAJ[2], Jack LANDY[3]

[1]*Earth System Science Interdisciplinary Center, University of Maryland, MD, USA*

[2]*Climate Research Division, Environment and Climate Change Canada, Toronto, Canada*

[3]*Earth Observation Group, Institute of Physics and Technology, UiT The Arctic University of Norway, Tromsø, Norway*

*Correspondence: Alek Petty <akpetty@umd.edu>*

**ABSTRACT. We present an initial assessment of all-season Arctic sea ice thickness estimates from ICESat-2 by combining freeboard retrievals with all-season SnowModel-LG snow loading. ICESat-2 captures the key regional and seasonal patterns of Arctic sea ice variability and shows good agreement with CryoSat-2 all-season estimates, including regional patterns of inter-annual variability in summer ice thickness. ICESat-2 shows consistently thicker ice compared to CryoSat-2 across the western coastal Arctic, while CryoSat-2 shows some periods of thicker ice across the Central Arctic, largely consistent with winter thickness biases. Validation against upward-looking sonar moorings, IceBird-2019 airborne observations, and MOSAiC buoy data highlights generally strong performance across a range of conditions, although seasonal biases linked to snow loading, freeboard differences, and ice density assumptions persist. The SnowModel-LG and NESOSIM snow accumulation models perform well across the validation datasets, but do not consistently add skill beyond the modified Warren climatology. Experimental ICESat-2/CryoSat-2 dual altimetry winter snow depths show strong performance relative to existing products and future work should extend these into summer for further assessments. Overall, our analysis supports the viability of an all-season ICESat-2-derived thickness record.**

## 1 INTRODUCTION

Monitoring Arctic sea ice from space is crucial for understanding our rapidly changing polar regions. Satellite observations provide arguably the best means to consistently track variability and trends in sea ice conditions due to their combination of reliability, basin-scale coverage and multi-year mission duration (Meier and others, 2014; Kwok, 2018; Stroeve and Notz, 2018). Satellite-derived sea ice observations are routinely used to assess and calibrate climate models (Notz and Stroeve, 2016; Massonnet and others, 2018), and understand the impacts of sea ice loss on global weather patterns (Cohen and others, 2014), ocean circulation (Polyakov and others, 2023) and Arctic ecosystems (Post and others, 2013).

NASA's ICESat-2 mission has significantly enhanced our ability to routinely monitor sea ice conditions at high resolution across the polar oceans (Markus and others, 2017). The data obtained from ICESat-2's Advanced Topographic Laser Altimeter System (ATLAS) over sea ice include estimates of height and total freeboard, the vertical extension of sea ice and its overlying snow cover above local sea level. The official ICESat-2 sea ice data products include along-track height (ATL07) and total freeboard (ATL10) for each of the six laser beams, as well as monthly gridded estimates of total freeboard (ATL20) and sea surface height anomalies (ATL21). These data are routinely updated and made available through the National Snow and Ice Data Center (NSIDC). ICESat-2's year-round data acquisition has provided a continuous record to monitor total freeboard variability since its launch in fall 2018 (Kwok and others, 2019b; Petty and others, 2023a,b). The along-track sea ice height and total freeboards have demonstrated high precision and accuracy compared to coincident airborne data collected in spring 2019 (Kwok and others, 2019a), with further validation across seasons and regions still on-going. ICESat-2 extends the laser altimetry record of sea ice obtained by the original ICESat mission (2003–2009) (Kwok and Cunningham, 2008; Petty and others, 2020) and provides a crucial complement to radar altimetry data obtained by the European Space Agency's (ESA) CryoSat-2 mission, which has been operational since its launch in 2010 (Kwok, 2018; Tilling and others, 2018; Ricker and others, 2017; Landy and others, 2022).

Estimates of winter Arctic sea ice thickness have been produced from ICESat-2 total freeboards using the traditional approach of assuming hydrostatic equilibrium and prescribing snow loading and ice density (Petty and others, 2023c). Both along-track (IS2SITDAT4 v1, Petty and others (2022)) and monthly gridded (IS2SITMOGR4 currently at v3, Petty and others (2023c)) datasets are made available through the NSIDC, with the monthly gridded dataset updated annually. These winter Arctic sea ice thickness estimates have primarily utilized snow loading estimates from the NASA Eulerian Snow on Sea Ice Model (NESOSIM) (Petty and others, 2018) to-date. Updates to NESOSIM (now at Version 1.1) and, more significantly, updates to the underlying ICESat-2 freeboards (Release 006 at the time of writing) have improved agreement with various CryoSat-2 winter Arctic sea ice thickness estimates (Kwok and others, 2021; Petty and others, 2023b). The thickness estimates are currently produced for the Arctic winter months only (September through April) due to the unavailability of NESOSIM snow loading in summer (no inclusion of summer melt processes to-date) and concerns around freeboard data reliability in summer, when melt ponds add uncertainty to the ICESat-2 surface classification and freeboard retrievals (Tilling and others, 2020). A summer airborne ICESat-2 cal/val campaign was undertaken in 2022, which included data collected by both the Land, Vegetation, and Ice Sensor (LVIS) and Leica Chiroptera-4x (CHIR) lidar systems (Saylam and others, 2025) as well as coincident georeferenced imagery (Blair and others, 2023). Preliminary results indicate encouraging performance of the summer ICESat2- height retrievals (Saylam and others, 2025), but no comprehensive evaluation of summer total freeboard has been undertaken to-date.

In contrast, recent advances in data processing techniques have enabled new all-season ice freeboard estimates from ESA's CryoSat-2 (Dawson and others, 2022), which have been combined with all-season Arctic snow loading estimates from the SnowModel-LG Lagrangian accumulation model (Liston and others, 2020) to produce all-season estimates of Arctic sea ice thickness (Landy and others, 2022). These data have provided crucial new insights into seasonal and regional thickness anomalies and forecast skill relevant to various Arctic stakeholders. In addition, new methods to derive snow depth and sea ice thickness concurrently by fusing altimetry data across missions/sensors, e.g. CryoSat-2's radar-derived ice freeboards and ICESat-2's laser-derived total freeboard, and leveraging their contrasting profiling assumptions is an active area of research focus and promise (Kwok and others, 2020; Kacimi and Kwok, 2022; Fredensborg Hansen and others, 2024; Landy and others, 2024; Carret and others, 2025).

In this study, we seek to extend the winter (September to April) ICESat-2 derived sea ice thickness estimates into summer and provide a first assessment of these data relative to the existing CryoSat-2 all-season estimates. We utilize the all-season snow loading estimates from SnowModel-LG to ensure consistency with the all-season CryoSat-2 product (Landy and others, 2022) and to provide clearer insights into the impact of altimetry differences on resultant sea ice thickness. Although summer freeboard validation is lacking, we instead carry out indirect validation by comparing the new all-season ICESat-2-derived thickness estimates with a variety of independent datasets: (i) under-ice upward-looking sonar (ULS) mooring ice draft data from the Beaufort Gyre Exploration Project (BGEP) (Krishfield and others, 2014), (ii) multisensor airborne data collected during the 2019 AWI IceBird campaign (Jutila and others, 2024), (iii) snow and ice thickness buoy observations collected during the MOSAiC expedition (Lei and others, 2022). The BGEP dataset has a strong legacy of supporting altimetry-derived Arctic sea ice thickness validation (Landy and others, 2022; Petty and others, 2023b) and provides consistent data across multiple years, however the moorings are limited to a fixed Beaufort Sea region. The MOSAiC and IceBird datasets provide crucial additional data across other regions of the Arctic, albeit limited in time. We include the CryoSat-2 all-season dataset, an experimental CryoSat-2/ICESat-2 derived winter Arctic dual altimetry fusion snow depth dataset (Landy and others, 2024) and additional input assumptions in our analysis and assessments to provide context for our all-season ICESat-2 thickness assessments. The overall objectives of this study are:

1. Incorporate SnowModel-LG all-season snow depth and density estimates into ICESat-2 thickness retrievals, providing an initial estimate of all-season ICESat-2 Arctic sea ice thickness.

2. Compare the new all-season ICESat-2 thickness results with the current state-of-the-art CryoSat-2 derived all-season thickness estimates.

3. Assess the new summer and existing winter ICESat-2 and all-season CryoSat-2 thickness estimates with independent Arctic snow depth and thickness datasets, highlighting the seasonal and regional biases across datasets.

4. Provide new insights into the performance of altimetry-derived Arctic sea ice thickness estimates and help motivate future development efforts.

All of the analysis presented in this study is provided publicly in a series of online interactive notebooks (`https://www.icesat-2-sea-ice-state.info`), extending the analysis that supported our winter thickness assessments (Petty and others, 2023b). The notebooks provide transparency and guidance on how to implement similar comparisons, as well as enabling interested users to implement different filtering or masking options as desired.

# 2 DATA AND METHODS

## 2.1 ICESat-2

### *2.1.1 IS2SITMOGR4 v3 winter Arctic monthly gridded sea ice thickness*

We use monthly gridded winter Arctic sea ice thickness estimates from ICESat-2 (IS2SITMOGR4, Version 3), described in Petty and others (2023b) and disseminated through the National Snow and Ice Data Center (NSIDC) (Petty and others (2023c), `https://nsidc.org/data/is2sitmogr4`). These thickness estimates are derived from ICESat-2 total freeboard measurements (Release 006 ATL10 data for IS2SITMOGR4 v3) and the hydrostatic equilibrium assumption using snow loading estimates from the NASA Eulerian Snow On Sea Ice Model (NESOSIM, Version 1.1) (Petty and others, 2018, 2023c), a constant bulk ice density of 916 kg/m³ and seawater density of 1024 kg/m³. Sea ice thickness is first calculated along-track for the three strong beams of ICESat-2, using an empirically-derived snow redistribution scheme described in Petty and others (2020). The along-track thickness data from the three strong beams are binned monthly to a 25 km x 25 km North Polar Stereographic grid across the entire Arctic. IS2SITMOGR4 v3 thickness estimates are available from November 2018 onward, covering the Arctic Ocean between September and April. The underlying ATL10 freeboards are limited to regions of ice concentration >50% based on daily passive microwave observations.

IS2SITMOGR4 v3 includes estimates of winter Arctic sea ice thickness derived with different input assumptions which we utilize here for basic insights into the impact and sensitivity of our comparisons to the choice of input assumptions: (i) SM-LG: SnowModel-LG snow depth and density (Liston and others, 2020) and the resultant winter sea ice thickness were included in the IS2SITMOGR4 v3 release. SnowModel-LG integrates ERA5 snowfall data (MERRA-2 estimates also available) with a Lagrangian snow accumulation scheme, accounting for blowing snow redistribution and wind-driven mass loss—processes that are not explicitly represented in NESOSIM; (ii) MW99: the Warren snow depth/density climatology (Warren and others, 1999), modified such that snow depth is halved over first-year ice (FYI). Although this climatology was compiled from observations collected several decades ago, it provides a useful additional comparison to the accumulation models, and in-situ surveys continue to suggest it can provide realistic snow distributions over mature FYI and multiyear ice (MYI) (Haas and others, 2017); (iii) J22: the variable empirical bulk ice density parameterization of, Jutila and others (2022), a function of the along-track ice freeboard (total freeboard minus snow depth).

### *2.1.2 IS2SITMOGR4S summer Arctic monthly gridded sea ice thickness*

To extend ice thickness retrievals across the summer months of May through August, we additionally here derive year-round sea ice thickness estimates using the SnowModel-LG snow depth and density (Liston and others, 2020) as in the winter data above. We use the exact same processing chain as in IS2SITMOGR4 v3, using a constant bulk ice density of 916 kg/m$^3$ and seawater density of 1024 kg/m$^3$ and the empirical snow redistribution scheme. The SnowModel-LG data are available publicly through to July 2021, which limits our resultant thickness dataset to the November 2019 to July 2021 time-period. Between June 25th and July 9th, 2019 ICESat-2 entered safehold mode due to a spacecraft anomaly, with no data collected during this period. After leaving safemode, the spacecraft was collecting data nominally, but had issues related to pointing, degrading the radiometry and lead finding performance. No ATL10 freeboard data were generated until nominal pointing resumed around July 25th, 2019. This is the longest period of missing ATL10 data in the ICESat-2 sea ice data record and is summarized in the ATL10 NSIDC Known Issues document (`https://nsidc.org/sites/default/files/documents/technical-reference/icesat2_atl07_atl10_known_issues_v006.pdf`). Considering the significant missing data, July 2019 was not processed or included in this study. As June 2019 only included six days of missing data, we include that month in our analysis but note the slight skew of representative date towards the start of the month. Preliminary browse images for June 2019 and 2020 are included in the Supplementary Material (Figs. S1 and S2) highlighting the slight difference in mean date of the gridded data.

In addition, we use monthly mean ice passive microwave-derived ice concentration from the NOAA/NSIDC Climate Data Record (CDR), version 4 (Meier and others, 2021), provided in both the IS2SITMOGR4 and IS2SITMOGR4S datasets.

For analysis of both the IS2SITMOGR4 and IS2SITMOGR4S data we use the provided interpolated/Gaussian smoothed variables as described in Petty and others (2023b), developed to reduce aliasing from uneven monthly sampling and to fill in gaps across small regions of missing data, including the 88 degrees North pole hole. For the interpolated/Gaussian smoothed variables not provided in either product, we apply the same interpolation processing in this analysis for consistency. A 50 % monthly sea ice concentration masking is still applied, as in the underlying freeboard data.

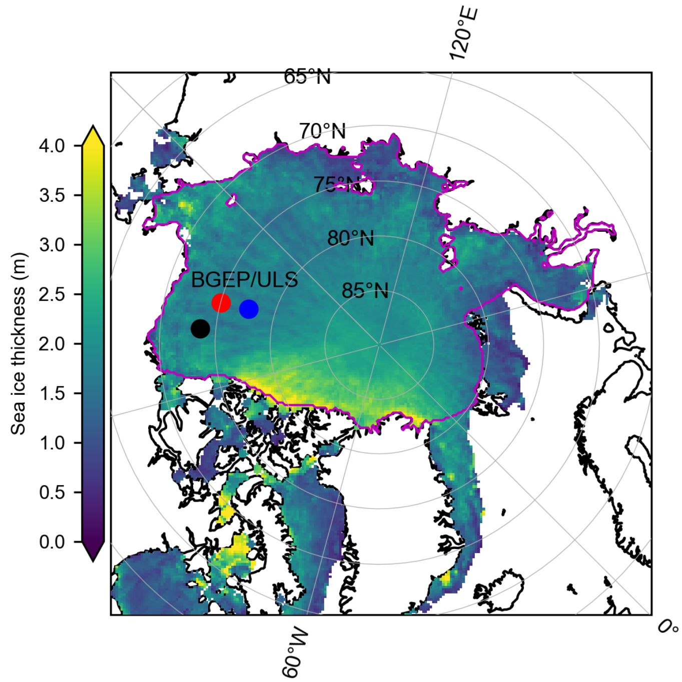


**Fig. 1.** Summer mean (May to August, 2019 to 2021) ICESat-2 sea ice thickness with SnowModel-LG snow loading, using the interpolated/smoothed data and filled in pole-hole. The red, blue and black circles show the location of the BGEP ULS moorings A, B and D respectively. The magenta contour shows the Arctic Ocean domain we use in our time-series analysis (Fig. 5).

---

## 2.2 CryoSat-2 all-season ice thickness

We use the University of Bristol (UBRIS) CryoSat-2 all-season sea ice thickness product, Version 1.0 (Landy and others, 2022) available from `https://data.bas.ac.uk/full-record.php?id=GB/NERC/BAS/PDC/01613`. This dataset provides biweekly gridded Arctic sea ice thickness estimates from October 2010 through to July 2021. The period of overlap, November 2018 to July 2021 permits multiple years of comparison with our ICESat-2 derived thickness estimates. Key differences between the CryoSat-2 and ICESat-2 thickness datasets include: (i) The UBRIS CryoSat-2 data have been generated with ice-age-dependent ice densities of 917 kg/m$^3$ (FYI) and 881 kg/m$^3$ (MYI). The NSIDC weekly 12.5-km sea ice age product V4 (`https://nsidc.org/data/nsidc-0611`)) was used to differentiate between zones of FYI and MYI. The differences in density for MYI between UBRIS and IS2SITMOGR4S could produce an offset in derived sea ice thickness, ii) The UBRIS CryoSat-2 data are posted biweekly which we resample here to monthly to be consistent with the monthly ICESat-2 data, iii) The UBRIS CryoSat-2 data are provided at a 80 km spatial resolution on an EASE2.0 grid. We regrid/downsample these to the 25 km Polar Stereographic grid of IS2SITMOGR4 to enable spatial comparison mapping, noting that the data still represents coarser grid-scales.

For the time series analysis we mask all ICESat-2 and CryoSat-2 data outside of an Arctic Ocean domain (includes the Central Arctic, Beaufort Sea, Chukchi Sea, E. Siberian Sea, Kara Sea) to avoid regions that are generally considered more uncertain (wave contamination, snow/flooding etc) and focus on the region where our input assumptions and validation data are more representative. The peripheral/masked regions are predominantly sea ice free in late-summer so this masking is more relevant for our winter analysis. In addition, when indicated we utilize a common masking approach, as in Petty and others (2023b), to ensure we only analyze grid-cells where both the ICESat-2/SM-LG thickness and CryoSat-2/SM-LG thickness are valid for the given month to mitigate against sampling differences between the products. Finally, in some of our spatial comparisons (as indicated) we additionally utilize perennial masking where we only show grid-cells that provide consistent data across all summer months in both IS-2 and CS-2 to further avoid sampling biases.

## 2.3 ICESat-2/CryoSat-2 winter Arctic dual altimetry fusion snow depths

We use preliminary winter Arctic snow depth estimates produced through the fusion of ICESat-2 total freeboards and CryoSat-2 ice freeboards, described in Landy and others (2024), with the data provided on Zenodo (`https://zenodo.org/records/13774843`). Validating these new multi-sensor data are not a primary focus of this study, but we incorporate these data here for added context regarding potential biases in our model-based snow depths and their potential role in driving differences between ICESat-2 and CryoSat-2 derived thicknesses. These data were generated using rel004 ICESat-2 monthly gridded ATL20 freeboards which use the same rel006 along-track ATL10 freeboards as in IS2SITMOGR4 v3 and IS2SITMOGR4S v1.

## 2.4 BGEP ULS ice drafts

The Beaufort Gyre Exploration Project (BGEP) provide upward-looking sonar (ULS) ice draft estimates from three moorings (A, B, and D, See Fig. 1) deployed across the Beaufort Sea (Krishfield and others, 2014). The data have been publicly available since the launch of ICESat-2 through currently to August/September 2023 (`https://www2.whoi.edu/site/beaufortgyre/data/mooring-data/`). Ice draft typically composes a more significant fraction of the total ice thickness compared to the freeboard measured by satellites, depending on the relative densities of ice, seawater and the overlying snow loading, making it a desirable validation metric. Individual ULS draft measurements are assumed to have a constant uncertainty of 10 cm (Krishfield and others, 2014). To compare with the satellite products, we first resample the provided ULS data to daily then monthly means. We then follow the approach of Petty and others (2023b) and take the mean of all valid ICESat-2 grid-cells within a certain radius of a given mooring, and compare this to the monthly mean ULS draft estimate. We use an averaging radius of 100 km in this study, as a compromise between the 50 km used in Petty and others (2023b) and the 150 km used in Landy and others (2022). Petty and others (2023b) explored the impact of averaging radius on BGEP/ULS comparisons and showed only minimal differences between 50 km and 150 km radii.

We calculate ice draft from the ICESat-2 data by simply adding snow depth to ice thickness and subtracting the total freeboard. The UBRIS CryoSat-2/SM-LG dataset does not include ice freeboard, so we instead estimate this using the hydrostatic equilibrium equation and the provided variables of bulk ice density, snow depth and density and seawater density.

## 2.5 MOSAiC buoy snow depths and ice thickness

The Multidisciplinary Drifting Observatory for the Study of Arctic Climate (MOSAiC) expedition (2019-2020) provided high-quality in-situ observations of Arctic sea ice (Nicolaus and others, 2022). We utilize snow depth and sea ice thickness measurements obtained from 19 snow and ice mass balance array (SIMBA) buoys deployed during the MOSAiC expedition (Lei and others, 2022) as independent validation data. SIMBA buoys are thermistor-string-type buoys from which air-snow, snow-ice, and ice-water interfaces may be detected, producing measurements of snow and sea ice thickness. The buoys were initially deployed over unponded level ice, and 10 of the buoys collected data for the entire sea ice growth season, providing overall observational coverage from October 2019 to July 2020 (Lei and others, 2022). The buoy tracks drifted from the Eastern Arctic (in October 2019) through towards Fram Strait (spring 2020). Absolute ice thickness and snow depth measurements from individual buoys are not necessarily representative of the average conditions of ice floes in the surrounding area; however, here we are able to benefit from the deployment of a dense network of buoys, which should improve the representation.

The buoy observations are highly localized in nature, so we bin them at daily timescales to a 100 km $\times$ 100 km North Polar Stereographic grid. The daily-aggregated data are resampled to monthly gridded means to compare with the monthly gridded satellite estimates. We coarsen the ICESat-2/CryoSat-2 data to the same 100-km resolution before undertaking our comparisons (we require at least four valid 25 km grid points for the 100 km coarsened mean to be used). 25 km gridded versions of the comparisons between buoys and satellite observations are included in the Supplementary Material as noted (generally showing worse statistical comparisons).

### 2.6 AWI IceBird-2019 snow depths and ice thickness

The Alfred Wegener Institute (AWI) IceBird campaign provides airborne measurements of sea ice thickness and snow depth using combined radar, lidar and (electromagnetic) EM-bird data fusion. We utilize sea ice thickness and snow depth estimates obtained from 5 single-day surveys in April 2019 (April 2, 4, 7, 8, and 10) across the western Arctic Ocean/Beaufort Sea, spanning both first-year and multiyear ice regimes (Jutila and others, 2024). We calculate sea ice thickness from the difference between the sea-ice-plus-snow thickness from electromagnetic induction sensor measurements and coincident snow depth measurements from snow radar data. We exclude measurements where data quality flags indicate negative freeboard, a low number of snow depth estimates within the EM sensor footprint, and implausibly low total thickness values (less than thickness uncertainty, snow depth, or snow freeboard). We bin these data daily to the coarser 100 km $\times$ 100 km North Polar Stereographic grid as discussed in the previous section, before generating a single April 2019 monthly gridded mean dataset. 25 km gridded versions are again included in the Supplementary Material as noted.

## 3 RESULTS

### 3.1 All-season sea ice thickness estimates

Fig. 2 shows the new summer (May to August) monthly mean Arctic sea ice thickness estimates derived from ICESat-2 total freeboards (rel006 ATL10) and SnowModel-LG snow loading (IS-2/SM-LG) for 2019, 2020, and 2021 using the interpolated/smoothed data on the 25 km x 25 km North Polar Stereographic grid. The IS-2/SM-LG summer thicknesses show regional distributions largely consistent with the winter freeboards and thickness, including thicker ice along the western Arctic coastline, but also localized regions of thicker ice within the eastern Arctic (Petty and others, 2023b). The expected seasonal decline is clearly evident across all three summers and spatial coverage appears consistent across months. The interpolated/smoothed data still show evidence of aliasing due to uneven monthly sampling, especially in

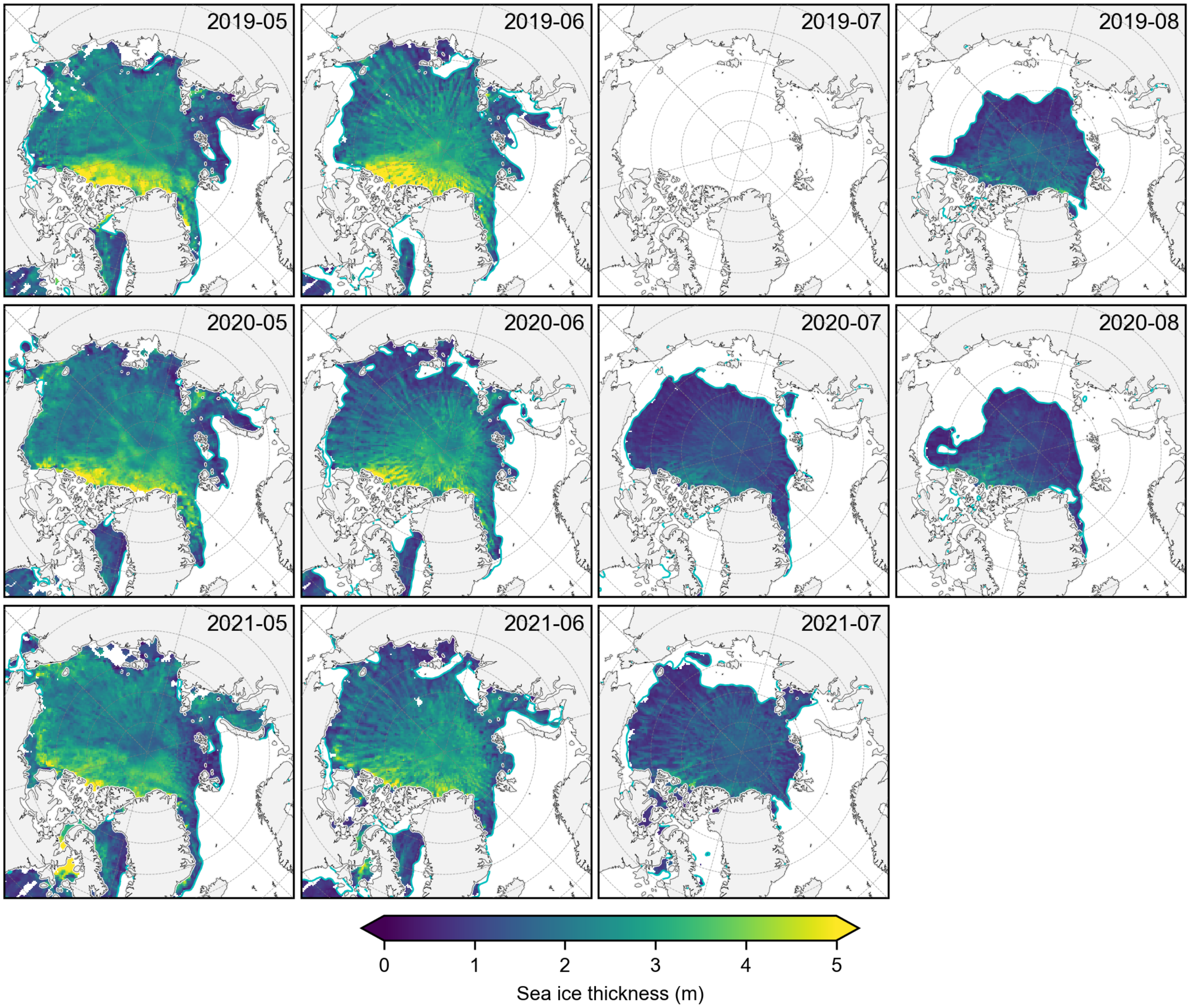


**Fig. 2.** Monthly mean summer (May through August, 2019 to 2021) ICESat-2 Arctic sea ice thickness estimates with SnowModel-LG snow loading, using the interpolated/smoothed gridded data. The cyan contour indicates the 50 % sea ice concentration from the monthly NSIDC CDR v4 dataset.

---

June when the sea ice conditions are changing most rapidly within the month. We discuss the need for enhanced gridding/interpolation in the discussion.

Fig. 3 shows spatial difference maps between the IS-2/SM-LG summer mean thickness estimates and the summer mean CryoSat-2/SnowModel-LG (CS-2/SM-LG, UBRIS) data. In these comparisons we use the perennial/common data masking introduced in Sect. 2.2 to only show grid-cells that provide consistent monthly coverage across both products to avoid monthly sampling biases contaminating the seasonal

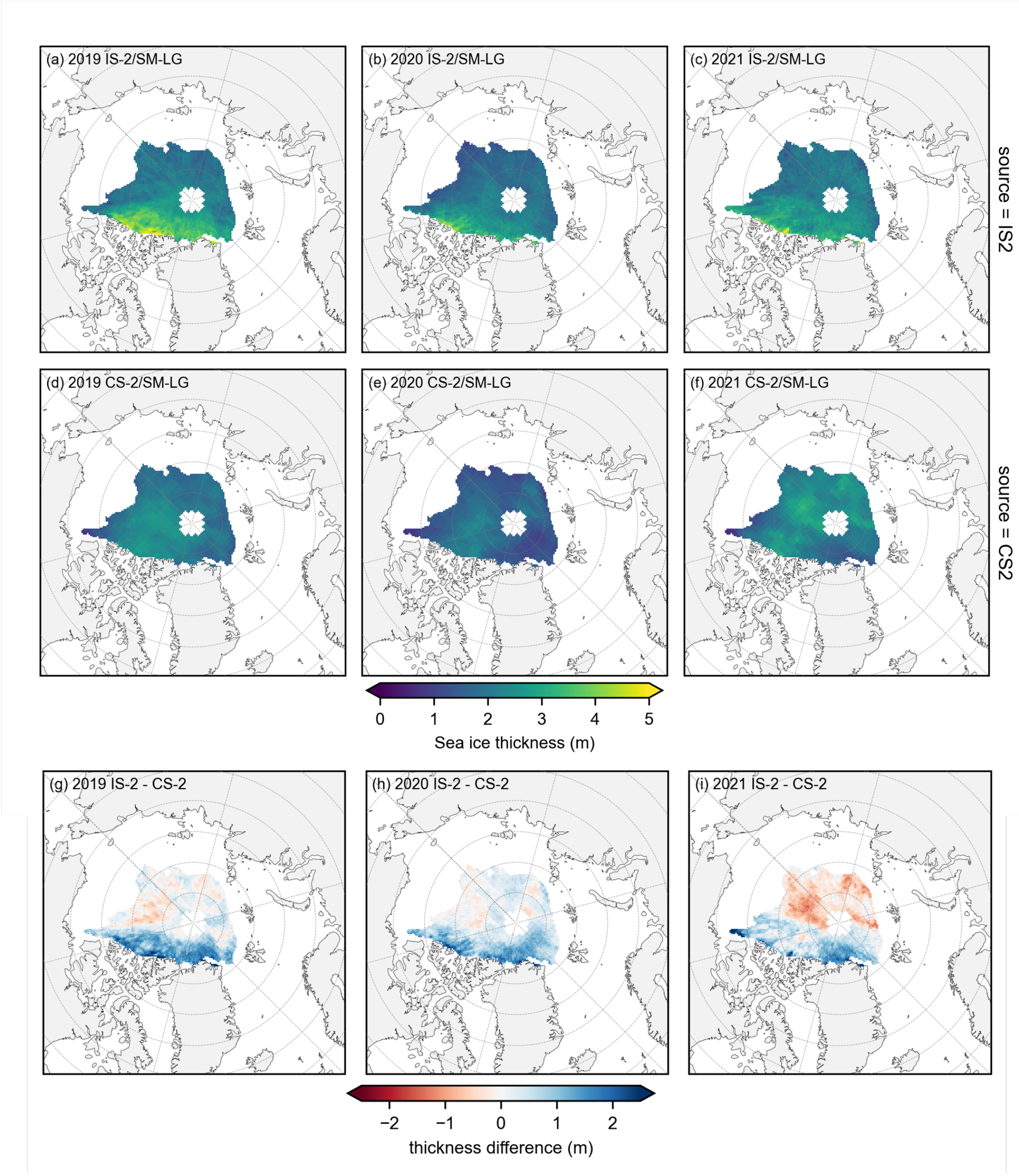


**Fig. 3.** Summer mean (May through August) monthly gridded sea ice thickness from (top row) ICESat-2 and SnowModel-LG (IS-2/SM-LG), (middle row) CryoSat-2 and SnowModel-LG (CS-2/SM-LG) and (bottom row) differences between IS-2 and CS-2 for 2019 (left), 2020 (middle) and 2021 (right). The monthly data only include grid-cells where both datasets show consistent monthly data across both datasets (a perennial common mask) before averaging. The 2019 means do not include July (missing IS-2 freeboards), while 2021 means do not include August (missing SM-LG).

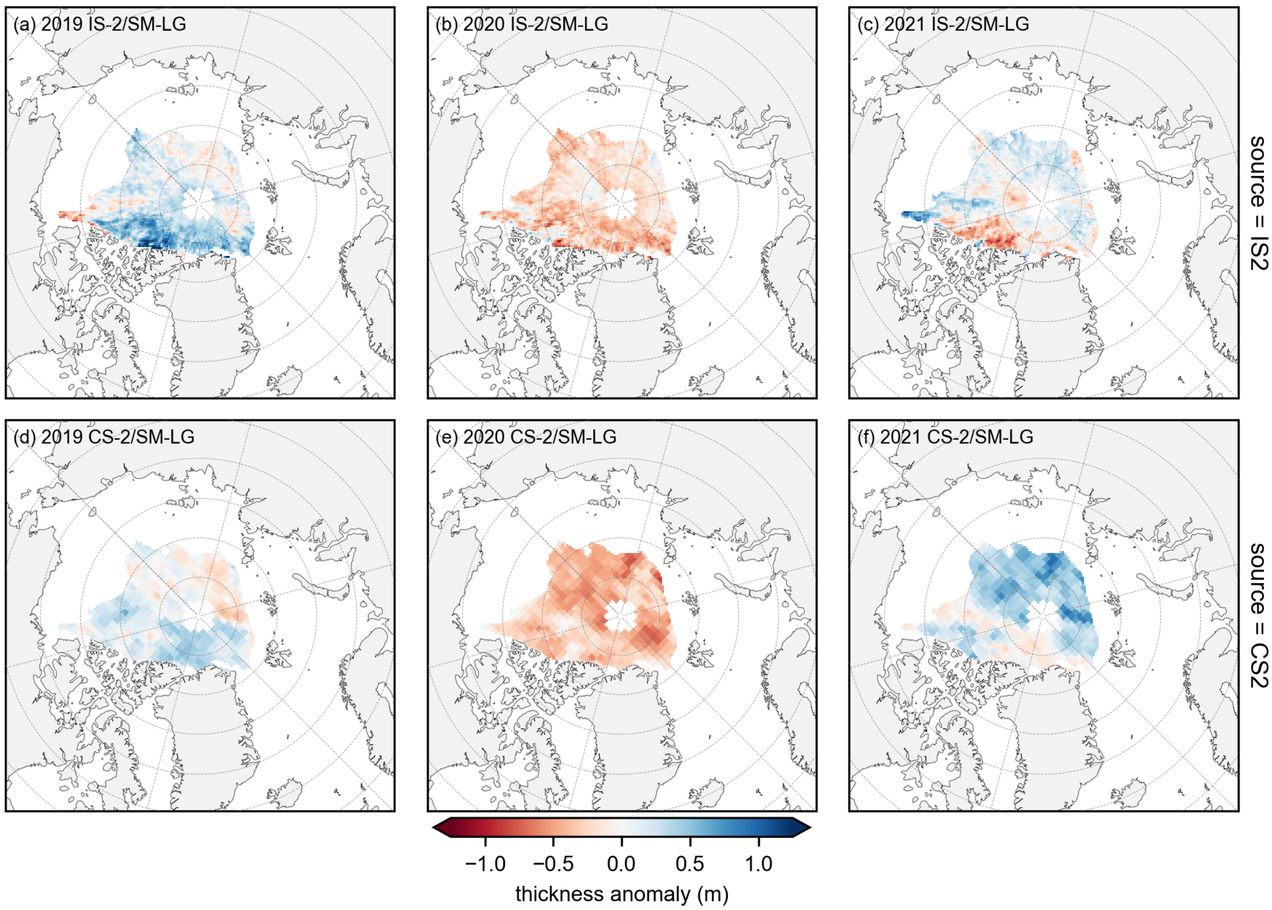


**Fig. 4.** Summer mean (May to August) sea ice thickness anomalies relative to the three year (2019 to 2021) summer means for (a - c) ICESat-2 and SnowModel-LG (IS-2/SM-LG) and (d - f) CryoSat-2 and SnowModel-LG (CS-2/SM-LG). The monthly data only include grid-cells where both datasets show consistent monthly data across both datasets (a perennial common mask) before averaging. The 2019 means do not include July (missing IS-2 freeboards), while 2021 means do not include August (missing SM-LG).

---

averaging (ICESat-2 applies a stricter 50 % sea ice concentration filter and also experiences more data drop-out in general). The use of seasonal means also reduces the aliasing issues discussed in the previous monthly analysis, with the monthly CS-2/SM-LG thickness and monthly difference maps provided in the Supplementary Material (Fig. S3 and S4). Overall, there is reasonable agreement between the IS-2 and CS-2-derived thickness estimates in terms of basin mean thickness but with significant regional differences of up to 1-2 m. IS-2/SM-LG shows consistently thicker ice compared to CS-2/SM-LG in all three summers across the western central Arctic, especially along the Greenland and Canadian Arctic coastline. However, IS-2 also shows some regions of thinner ice compared to CS-2 further to the North/East of the Arctic, especially in 2021. The monthly difference maps (Supplementary Material, Fig. S4) also show significant regions in May/June where IS-2 is 1-2 m thinner than CS-2 across the southern Beaufort/Chukchi seas, and up to 2 m thicker than CS-2 in the northern Kara Sea region. While not the main focus of this study, we also produced winter (January through April) IS-2 to CS-2 thickness differences, which show similar regional thickness biases to summer (Supplementary Material Fig. S5). Similar regional winter IS-2/CS-2 thickness biases were also present in comparisons with other CryoSat-2 derived thickness products, as featured in the interactive analysis (`https://www.icesat-2-sea-ice-state.info/content/3_comparisons_with_cryosat-2_and_piomas.html`) associated with recent IS-2 winter thickness assessments (Petty and others, 2023c).

Fig. 4 shows the summer thickness anomalies relative to the three-summer mean for IS-2/SM-LG and CS-2/SM-LG. Both estimates show good agreement on the key inter-annual summer thickness anomaly patterns, e.g. the broad negative anomaly in the 2020 summer and the broad regions of competing negative/positive anomalies in 2019 and 2021, with some small differences at more local-scales. Despite the use of a common 25 km grid size in this analysis, the native resolution of the CS-2/SM-LG data is 80 km, which is one likely reason why the CS-2 anomalies show less grid-scale variability than IS-2. The strong consistency in inter-annual summer thickness anomalies, despite the short overlapping record, is encouraging.

Fig. 5 shows the seasonal time-series comparison of Arctic sea ice thickness from both IS-2 and CS-2 SM-LG all-season thickness estimates, as well as the official winter (September to April) IS2SITMOGR4 v3 product based on NESOSIM v1.1 snow loading (IS-2/NSIM). In this analysis we use all data within an Arctic Ocean region shown in Fig. 1 and a common (not perennial) masking to ensure each month we only use data for all variables shown where both IS-2/SM-LG and CS-2/SM-LG provide data. Fig. 5b also shows the monthly sea ice thickness anomalies of the two IS-2 thickness estimates relative to CS-2/SM-LG. Associated metrics of monthly mean snow depth, snow density, bulk ice density and ice concentration from various sources as noted are given in panels c to f. Overall, the IS2/SM-LG and CS-2/SM-LG all-season products show good agreement in terms of the seasonal cycle ($r = 0.89$), but with IS-2/SM-LG thicker than CS-2/SM-LG for most of the common time-period shown (mean bias of 31 cm). Both products capture a slight thinning between September and November as FYI begins to form and coverage expands across our Arctic Ocean study region (note the concentration increase in panel f). They also both show consistent

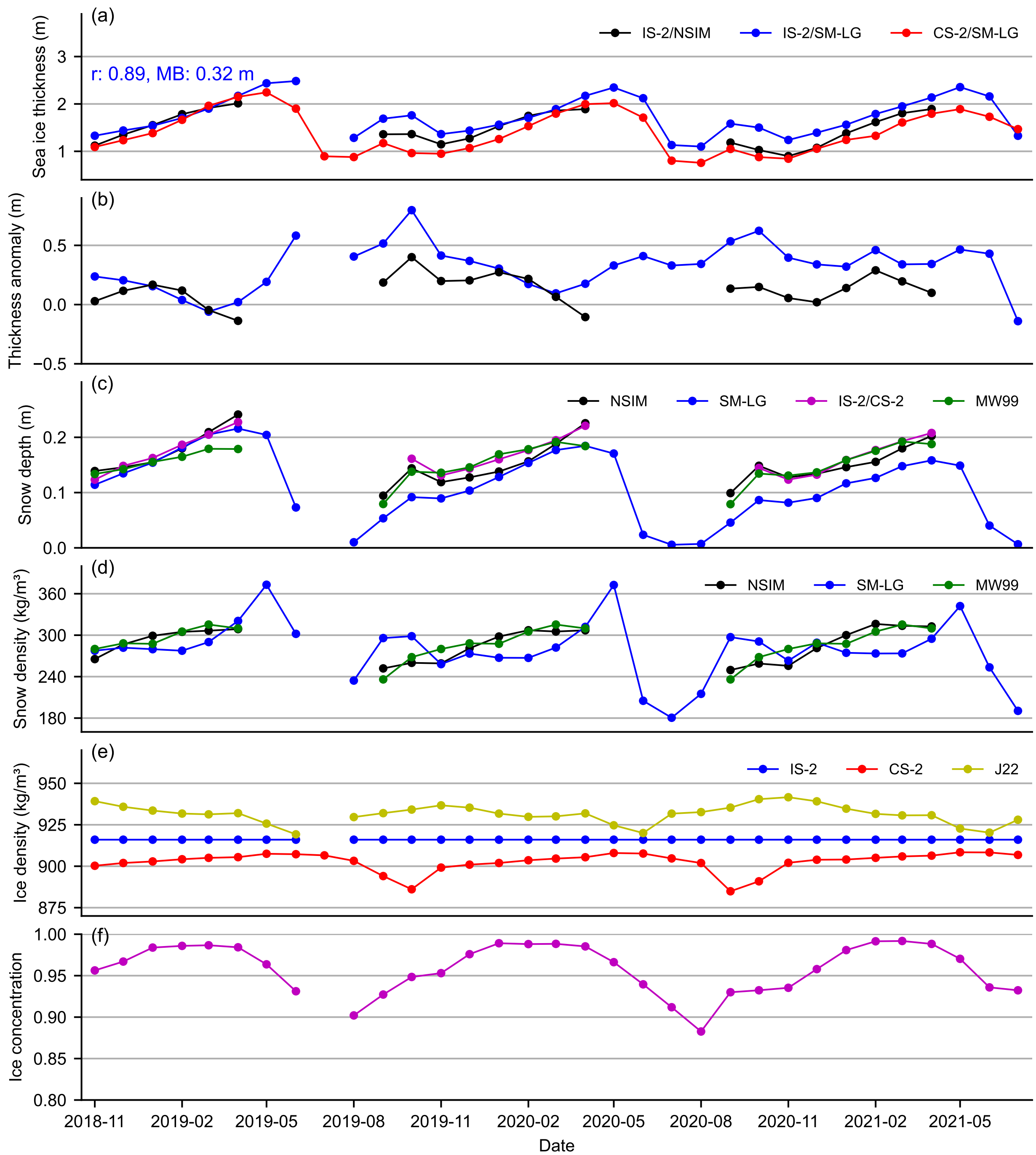


**Fig. 5.** Three years (November 2018 to July 2021) of (a) monthly Arctic sea ice thickness from IS2SITMOGR4 v3 with NESOSIM v1.1 snow loading (IS-2/NSIM, winter), ICESat-2 with SnowModel-LG (IS-2/SM-LG, all-season) and CryoSat-2 with SnowModel-LG (CS-2/SM-LG, all-season), (b) thickness anomalies relative to CS-2/SM-LG, (c) snow depths from NSIM and SM-LG (sub-sampled/gridded by IS-2), dual altimetry fusion snow depths (IS-2/CS-2), the modified Warren snow climatology (MW99), (d) snow density from NSIM, SM-LG and MW99, (e) bulk ice density assumptions used in IS-2, CS-2 and the J22 parameterization using IS-2/SM-LG data, (e) ice concentration from passive microwave (monthly NSIDC CDR v4 data). All data are first masked outside of an Arctic Ocean region shown in Fig. 1, and an additional common masking is applied each month, with monthly grid-cells masked if not included in both IS-2/SM-LG and CS-2/SM-LG datasets for the given month. No July 2019 estimates are available from IS-2 as detailed in Sect. 2.1.

thickening between November and April/May and a thickness decline between May or June (depending on the year and product) and August. IS-2/SM-LG generally exhibits a faster rate of summer thickness decline between June and July than CS-2/SM-LG. The IS-2/NSIM winter thickness estimates generally fall between the two SM-LG-derived thickness estimates, with all three products showing the best agreement in the early part of the coincident time-period (2018-11 to 2019-04). The winter IS-2/NSIM thicknesses are on average ∼10 - 20 cm thicker than CS-2/SM-LG, especially earlier in the winter season, while the all-season IS-2/SM-LG results are 31 cm thicker on average, but with strong seasonal variability. While the focus of this study was incorporating the new summer (May through August) data, some of the biggest monthly differences manifest during the fall freeze-up period and should be an area of future focus.

The strong agreement in the first winter season, and the middle of the second winter season (January to March 2020), is noteworthy for being the periods when SM-LG snow depths show the best agreement with NESOSIM and the two other provided snow depth estimates (IS-2/CS-2 and MW99). This provides some qualitative evidence of consistency between the IS-2 and CS-2 freeboard retrievals in the absence of significant snow biases. The SM-LG snow depths show a clear decrease in the subsequent two winters, which is not observed in the NESOSIM, IS-2/CS-2 or MW99 snow depths. The strong consistency in these three snow depth products provides some limited evidence of a potential negative bias in SM-LG in the later part of this time-period, which coincides with months of more significant thickness disagreement. Errors in snow depths contribute in an approximately opposing manner to laser vs radar freeboard-to-thickness conversion, driving thickness differences even in the absence of any freeboard bias in either product. For example, a low snow depth bias would produce a positive IS-2 thickness bias but a negative CS-2 thickness bias, which we discuss more later. Significant thickness differences are also observed between the IS-2 and CS-2 products using the same SM-LG snow loading during the non-winter months. Between May and early-July there is still a significant snow load on the ice, so we can assume that any winter bias in the snow loading (for any product) would extend into spring and summer. However, in the late summer the lack of snow cannot help to explain the biases between IS-2 and CS-2 thickness estimates.

Another notable feature is the strength of the mid-summer snow/thickness decline, however the lack of July 2019 IS-2 data complicates this assessment. The SM-LG snow depths show rapid thinning between May and June across all three summers (e.g. ∼22 cm in May 2019 to ∼8 cm in June). In 2019 this contributes to high June IS-2/SM-LG thicknesses, but reduced CS-2/SM-LG thicknesses based on the contrasting impact of snow depth on freeboard-thickness conversion for total vs ice freeboard data.

Subsequent years show more mixed impacts of this rapid snow decline, with additional analyses suggesting an overestimation of the seasonal cycle in the CS-2/SM-LG data (Song and others, 2024).

Snow density differences are clearly notable between SM-LG and NESOSIM/MW99, with SM-LG showing lower densities in winter, but snow density increasing to >360 kg/m$^3$ in May before declining rapidly to ∼200 kg/m$^3$ in June through August. Snow density generally provides only a second order impact on thickness and is thus not considered a major driver of the thickness differences observed, but is worth considering in future development and inter-comparison efforts. Finally, Fig. 5e shows the different bulk ice density assumptions used in IS-2/SM-LG and CS-2/SM-LG as well as a new bulk ice density estimate based on the J22 parametrization and our IS-2 freeboards, as discussed in Sect. 2.1. The CS-2 ice type density assumption (a lower density for multiyear ice) results in mean densities of ∼900 kg/m$^3$ compared to the constant value of 916 kg/m$^3$ in IS-2, reducing further in summer when the ice is mostly composed of remnant MYI. This density difference could also be driving a considerable fraction of the IS-2/SM-LG and CS-2/SM-LG thickness differences, if either product adopted the alternative bulk ice density assumption that would increase/decrease resultant ice thickness and reduce the overall bias by 20-30 cm on average. The J22/IS-2 bulk ice density parameterization output of ∼920-940 kg/m$^3$ provides an alternative estimate of higher densities than the current assumptions used in either primary IS-2 or CS-2 thickness products, which drive higher thicknesses across both datasets. However, this new bulk ice density parameterization was developed with multi-sensing airborne data collected in spring within limited campaigns across the Western Arctic only, and thus needs to be further validated across different regions and time-periods.

## 3.2 Comparisons with independent data

We next provide a series of independent data assessments to add insight into the accuracy of the various satellite-dervied products, including data from Upward Looking Sonar (ULS) mooring ice draft observations from the Beaufort Gyre Exploration Project (BGEP), snow and ice thickness buoy observations deployed during the 2019-2020 MOSAiC expedition, and snow and ice thickness airborne observations from the 2019 AWI IceBird campaign.

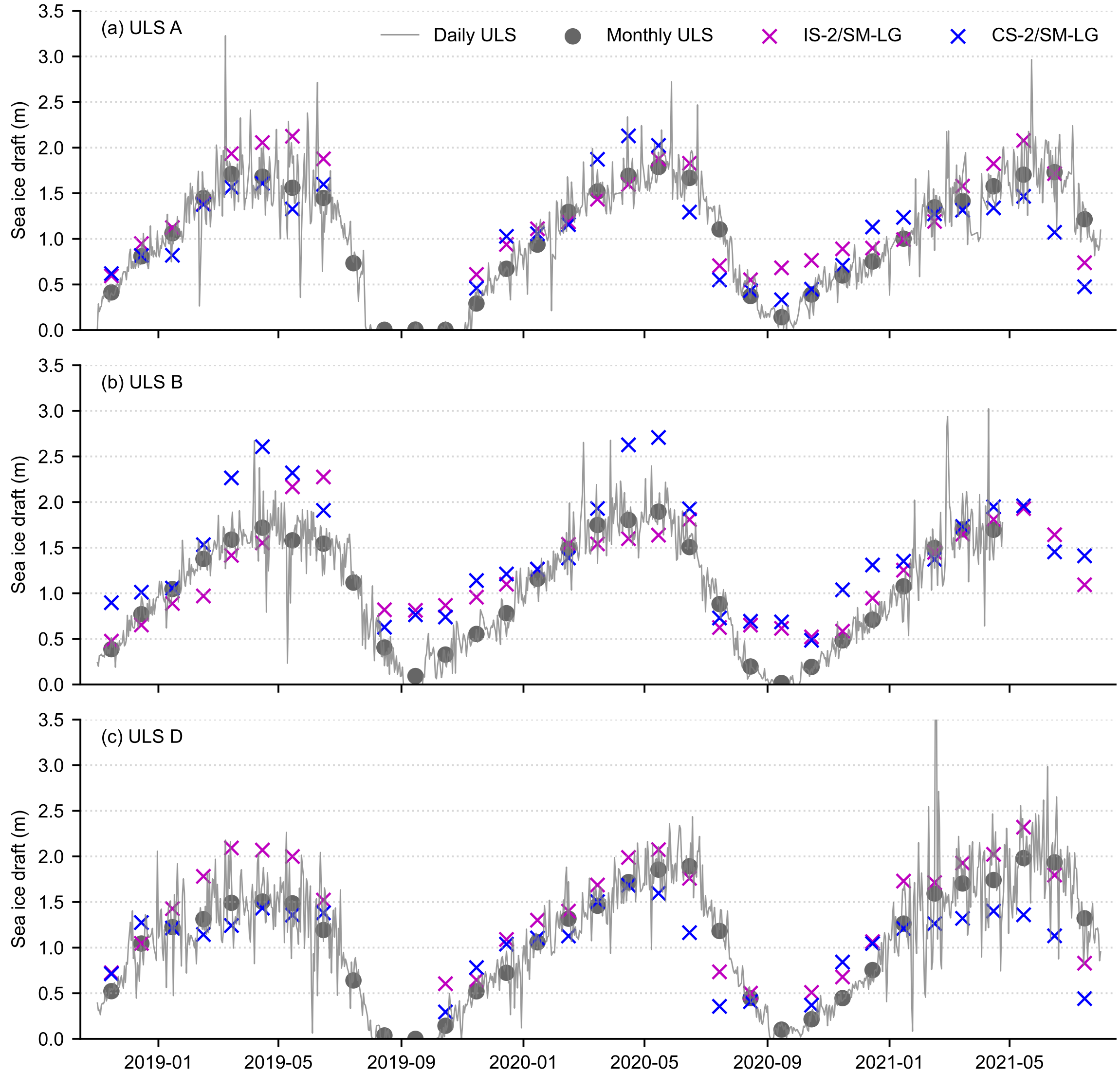


**Fig. 6.** Three year time-series comparison between Beaufort Gyre Exploration Project (BGEP), Upward Looking Sonar (ULS) ice draft measurements (daily and monthly means) and coincident ICESat-2/SnowModel-LG (IS-2/SM-LG) and CryoSat-2/SnowModel-LG (CS-2/SM-LG) derived ice draft at the three different BGEP mooring locations shown in Fig. 1.

### *3.2.1 BGEP ULS*

Fig. 6 shows a comparison of monthly mean BGEP ULS ice drafts with our satellite-derived ice draft estimates for both IS-2/SM-LG and CS-2/SM-LG all-season data. Some months in Fig. 6 are missing satellite-derived data due primarily to reduced summer ice coverage (the moorings are located close to the summer ice edge, IS-2 and CS-2 processing filters data with ice concentration below 50% and 30%

respectively). Both IS-2/SM-LG and CS-2/SM-LG capture the overall seasonal cycle of ice draft and the broad regional differences across the three moorings (all still within the Beaufort Sea). However, higher IS-2/CS-2-derived ice drafts are clearly evident during late-summer/early months over ULS mooring B and high CS-2/SM-LG-derived ice drafts are observed in some winter months, also over ULS mooring B. 2021 winter/spring is also notable for showing high biases in IS-2/SM-LG vs low biases in CS-2/SM-LG compared to mooring D and A to a lesser extent, the period when SM-LG was highlighted previously as showing a negative snow depth bias compared to the other snow products. This again alludes to the possible role of biases in snow depth driving the biases between the satellite-derived ice drafts with the moorings, since snow depth is the only variable of the hydrostatic equation that impacts ice thickness in contrasting directions for ICESat-2 and CryoSat-2 as discussed earlier.

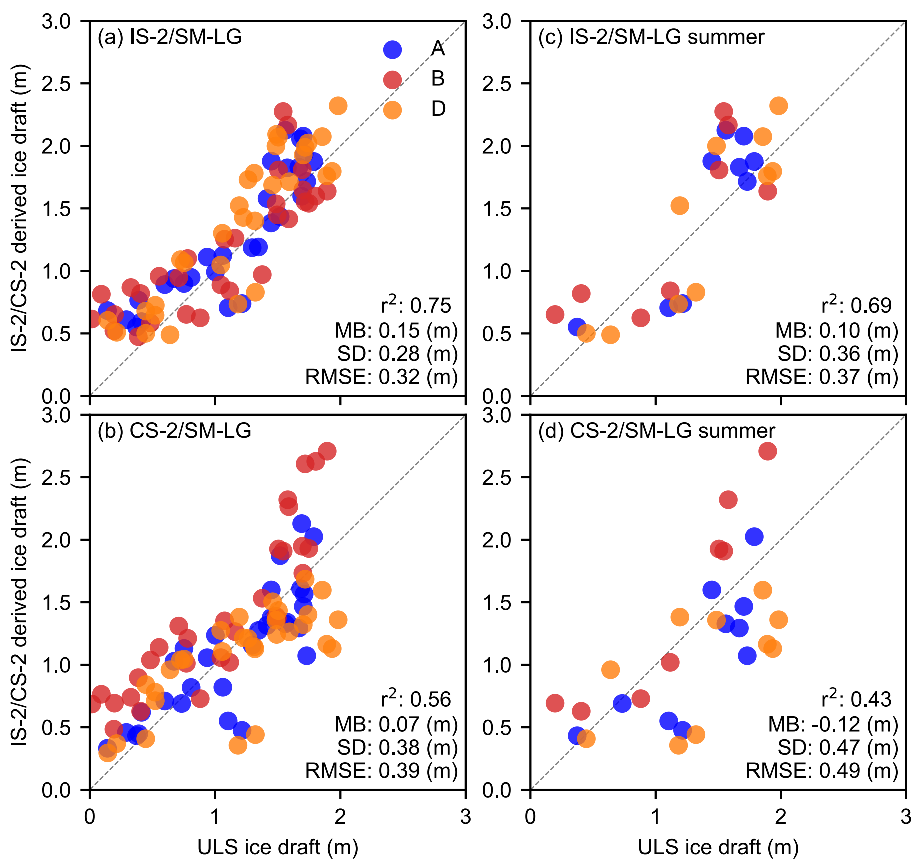


**Fig. 7.** Scatter plot comparisons of monthly mean Beaufort Gyre Exploration Project (BGEP), Upward Looking Sonar (ULS) ice draft measurements and coincident (a) ICESat-2/SnowModel-LG (IS-2/SM-LG) and (b) CryoSat-2/SnowModel-LG (CS-2/SM-LG) ice draft for the three different BGEP mooring locations from the time-series shown in Fig. 1. Panels (c) and (d) show data for the May to August summer months only. Statistics show the coefficient of determination $r^2$, mean bias (MB), standard deviation of differences (SD), root mean squared error (RMSE).

To better highlight the differences between the satellite-derived ice drafts and ULS ice drafts, Fig. 7a and b represents the same data as scatter plots with relevant statistical metrics included. The agreement with ULS is generally stronger for IS-2/SM-LG compared to CS-2/SM-LG, with lower root mean squared errors (RMSEs) for IS-2/SM-LG (0.32 m) compared to CS-2/SM-LG (0.39 m) and higher IS-2/SM-LG correlations ($r^2$ = 0.76) compared to CS-2/SM-LG ($r^2$ = 0.56). The mean bias (MB) is higher for IS-2/SM-LG (0.16 m) compared to CS-2/SM-LG (0.07 m), however, and these biases appear to manifest at both the high and low end of the distribution. CS-2/SM-LG features stronger spread across the distribution, hence the larger standard deviation of differences (0.39 m compared to 0.28 m). The high correlations primarily reflect the ability of IS-2/CS-2 to capture the significant seasonal cycle in thickness/draft, as this is the largest signal in these data. Note that similar comparisons for CS-2/SM-LG over the longer 2010 to 2021 period were provided in (Landy and others, 2022), with the longer time period enabling an increased focus on sub-seasonal thickness skill. Additional years of IS-2 data will help enable similar sub-seasonal skill assessments.

In Fig. 7c and d we show the same ULS comparisons for summer months only (May through August). The correlations decrease slightly for both products, although not significantly ($r^2$ = 0.67 for IS-2/SM-LG and 0.42 for CS-2/SM-LG). The RMSE increases to 0.38 m (IS-2/SM-LG) and 0.51 m (CS-2/SM-LG) and mean bias shows a slight reduction for IS-2/SM-LG (0.12 m), and small increase for CS-2/SM-LG (-0.14 m) relative to the all-season comparisons. The IS-2/SM-LG summer metrics are encouraging and suggests positive skill in IS-2 for sub-seasonal/inter-annual summer sea ice thickness assessments. The more limited summer data availability and the presence of these moorings near to the summer ice edge means we advise caution when interpreting these results.

To provide additional insight into the existing winter ICESat-2 thickness estimates (IS2SITMOGR4 v3) and their sensitivity to our chosen input assumptions, Fig. 8 shows winter comparisons using IS-2 thickness derived with different input assumptions, including MW99 snow loading and J22 ice density (with the NESOSIM v1.1 snow loading). We provide these to give more context to our assessments and to highlight the sensitivity of our results to plausible input assumptions. Currently, the MW99 and NSIM/J22 derived thicknesses are only available in the winter IS2SITMOGR4 v3 product, hence the more limited focus of this comparison. Note that while we call this winter, it includes data from September to April which still includes a significant seasonal cycle, driving much of the expected skill (Nab and others, 2024).

The RMSE values range from 0.19 m (IS-2/MW99) to 0.33 m (CS-2/SM-LG), with the IS-2/MW99

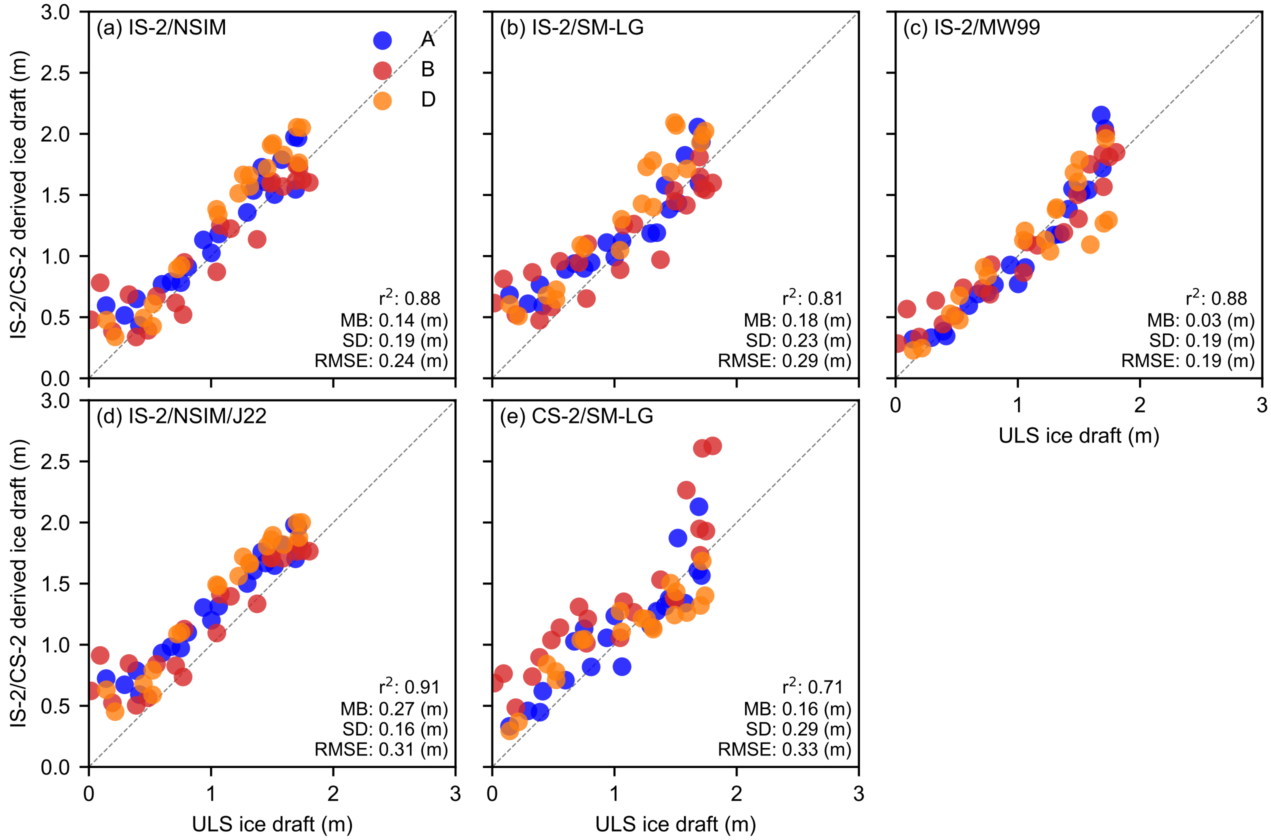


**Fig. 8.** As in Fig. 7 but showing winter data (September through April) for ICESat-2 with four different input assumptions, (a) NESOSIM v1.1 snow loading as in IS2SITMOGR4 v3 (b) SnowModel-LG (SM-LG) snow loading, (c) MW99 snow loading (d) NSIM snow loading and J22 bulk ice density, and (e) CryoSat-2/SM-LG data.

---

performance notably strong (also a 0.03 mean bias). The correlations are highest for the IS-2 freeboards and NESOSIM (0.88), MW99 (0.88) and NESOSIM combined with J22 ice density (0.91). The IS-2/NSIM/J22 comparisons, despite showing the highest correlations, also produce the highest mean bias (0.27 m) compared to the other comparisons. The comparisons with IS2 or CS2 and SM-LG show weaker correlations than for NSIM or MW99 snow loading. The CS-2/SM-LG comparisons are slightly weaker than IS-2/SM-LG, with a slightly larger mean bias (0.16 m) and RMSE (0.33 m), driven in-part by a few anomalously high ice drafts over the northernmost Mooring B. All the satellite-derived ice draft estimates struggle to capture the thin ice drafts, especially the IS-2/SM-LG and IS-2/NSIM data, suggesting possible issues with positive snow depths biases over thinner ice in the fall freeze-up period, as was also shown in Fig. 6.

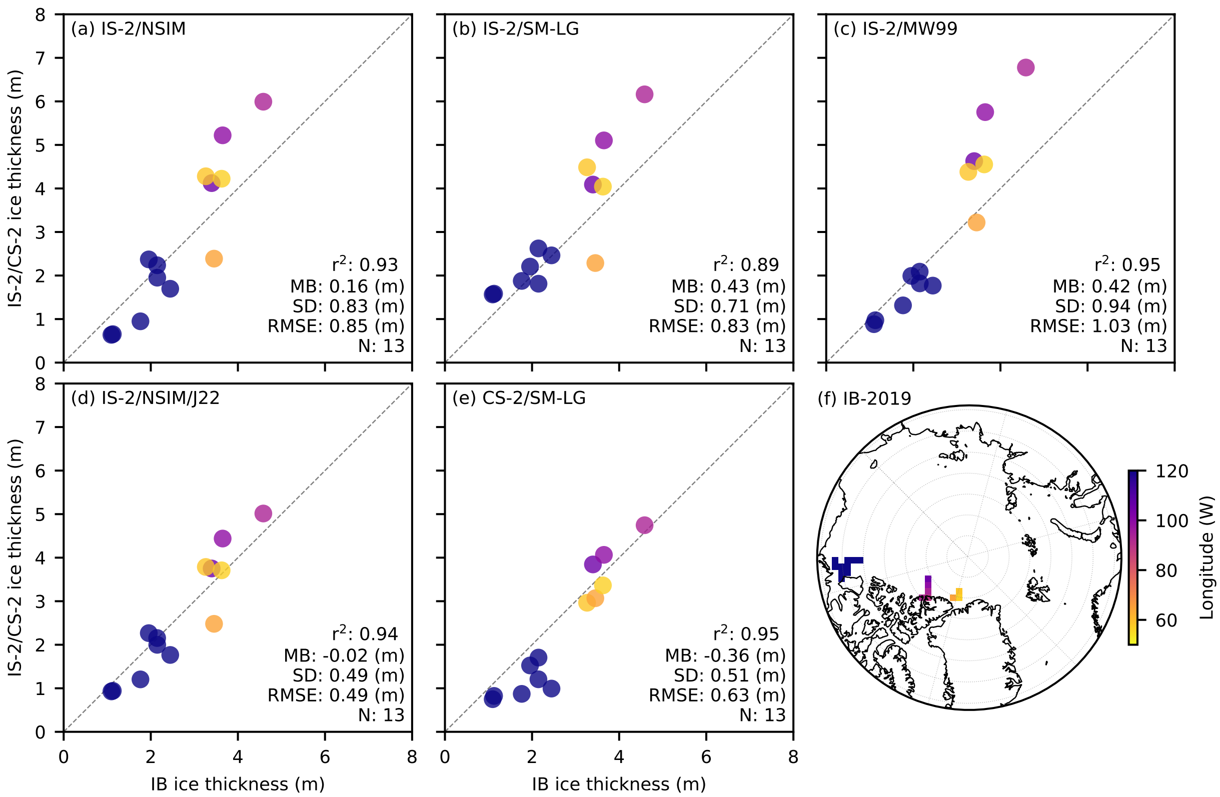


**Fig. 9.** Comparison of IceBird airborne ice thickness estimates in April 2019 (binned to a 100 km North Polar Stereographic grid) and coincident monthly mean 100 km coarsened ice thickness from ICESat-2 with four different input assumptions (a) NESOSIM v1.1 snow loading as in IS2SITMOGR4 v3 (b) SnowModel-LG snow loading (SM-LG), (d) modified Warren snow loading (MW99), (e) NSIM snow loading and J22 bulk ice densities and (f) CryoSat-2/SM-LG data. Panel (f) shows the IceBird 2019 flight-lines color-coded by longitude, which are used in the colors across all scatter plots.

---

### *3.2.2 AWI IceBird-2019*

In Fig. 9 we compare April 2019 IceBird thickness estimates with coincident monthly mean thickness from ICESat-2 using four different input assumptions as well as CryoSat-2/SM-LG. In this analysis the data are binned or coarsened to the 100 km x 100 km North Polar Stereographic grid as discussed in Sect. 2, resulting in only 13 grid-cells for comparison. 25 km versions are available in the Supplementary Material (Figs. S6 and S7), showing similar/worse comparison metrics. All products reproduce the large-scale spatial gradients observed by IceBird-2019, with correlations high across all products ($r^2 \sim 0.89$). IS-2/NSIM/J22 results in the lowest mean bias (–0.02 m) and RMSE (0.49 m) of all thickness estimates, however this is not a truly independent validation as the density parameterization was developed in-part using the same IceBird data presented here. The CS-2/SM-LG product shows good agreement over the thicker ice north of Greenland/Canadian Arctic, but a negative bias over the thinner ice profiled over the Beaufort Sea. The IS-2 products tend to exhibit positive thickness bias in the thicker ice north of Greenland/Canadian Arctic, but show better agreement in the thinner ice of the Beaufort Sea.

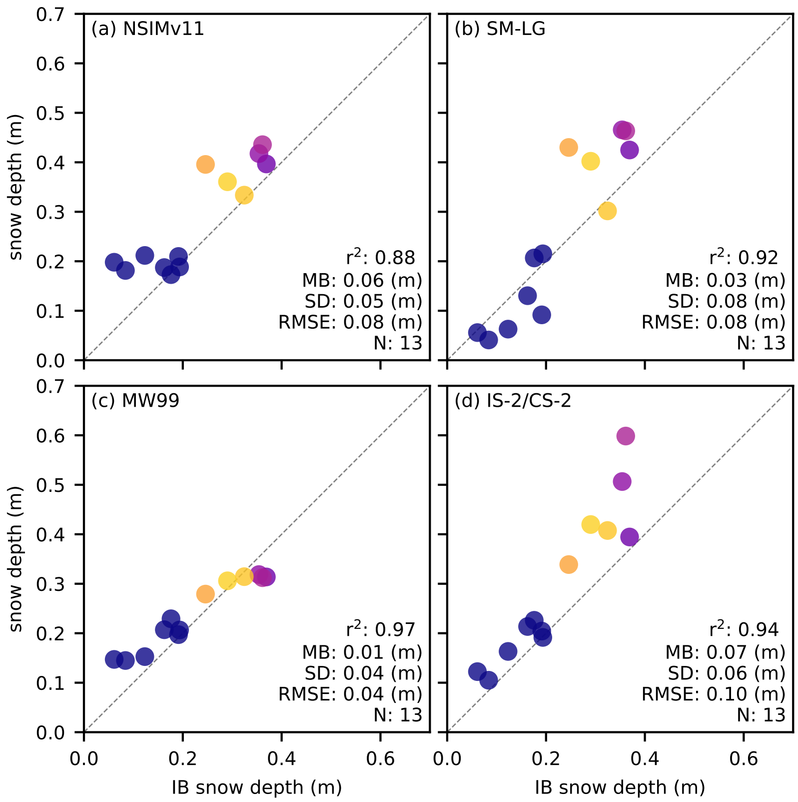


**Fig. 10.** Comparison of IceBird airborne snow depth estimates in April 2019 (binned to a 100 km North Polar Stereographic grid) and coincident monthly mean coarsened snow depths (sub-sampled by ICESat-2) from (a) NESOSIM v1.1 snow loading (NSIM) (b) SnowModel-LG snow loading (SM-LG), and (c) modified Warren snow loading (MW99) and (d) dual altimetry fusion snow depths (IS-2/CS-2). Scatter colors are based on the flight locations shown in Fig. 9.

---

In Fig. 10 we compare the IceBird-2019 derived snow depths and four snow products, NSIM, SM-LG, MW99 and also the preliminary IS-2/CS-2 dual altimetry fusion estimates. The correlations are again very high ($r^2$>0.88), with mean biases ranging from 0.01 (MW99) to 0.07 (IS-2/CS-2) and RMSE values ranging from 0.04 m (MW99) to 0.10 m (IS-2/CS-2). The performance of the MW99 snow depths (and resultant sea ice thickness shown in Fig. 9c) is notably high, however the snow depths do not capture the full-range of snow conditions observed by IceBird-2019 (∼14 to 32 cm for MW99 compared to ∼4 to 40 cm for IceBird) which we might expect from a climatology product. The IceBird-2019 flights cover regions expected to be broadly representative of the MW99 regional distribution based on the original station locations (Warren and others, 1999). While SM-LG and NSIM were able to simulate higher snow depths north of the Canadian Arctic, only SM-LG simulated the lower snow depths observed by IceBird-2019 over the Beaufort Sea. The IS-2/CS-2 dual altimetry fusion snow depths show encouraging performance overall, especially at the lower end of the distribution, but include a few abnormally high snow depths in the region north of Greenland/Canadian Arctic which reduce overall performance. This could be caused by biases in either or both the IS-2 and CS-2 freeboard observations; however, the results do not point towards partial penetration of the CS-2 Ku-band radar signal into the snow, which would lead to underestimated satellite snow depths.

#### *3.2.3 MOSAiC SIMBA buoys*

In Fig. 11 we compare the MOSAiC/SIMBA buoy-derived thicknesses with coincident monthly mean thicknesses from ICESat-2 using four different input assumptions as well as CryoSat-2/SM-LG. The data are again binned or coarsened to the 100 km x 100 km North Polar Stereographic grid. 25 km versions are available in the Supplementary material (Fig. S8 and S9), showing similar/worse comparison metrics. Here the data are also delineated into October to April 'apr' comparisons based on availability of auxiliary data with different input assumptions, and the full October to June 'all' MOSAiC/SIMBA data range (for both SM-LG-based thickness estimates), resulting in 35 and 46 grid-cells for comparison respectively. Overall, all products show good skill in capturing the combined seasonal and regional variability in ice thickness along the MOSAiC/SIMBA track, with correlations generally strong across all products ($r^2$=0.67 to 0.80). The RMSEs are relatively low, ranging from 0.30 m (IS-2/NSIM) to 0.52 m (both longer period SM-LG products), with mean biases of 0.12 m (IS-2/NSIM) to 0.43 m (IS-2/SM-LG through April). The introduction of the May/June data does not cause any notable impact on the comparison metrics. Unlike the previous analyses, the use of J22 densities does not result in improved agreement (the RMSE instead increases from 0.30 m to 0.38 m).

In Fig. 12 we show comparisons between the MOSAiC/SIMBA buoy-derived snow depths and the four snow products, NESOSIM v1.1, MW99, IS-2/CS-2 and SnowModel-LG for both the same October to April

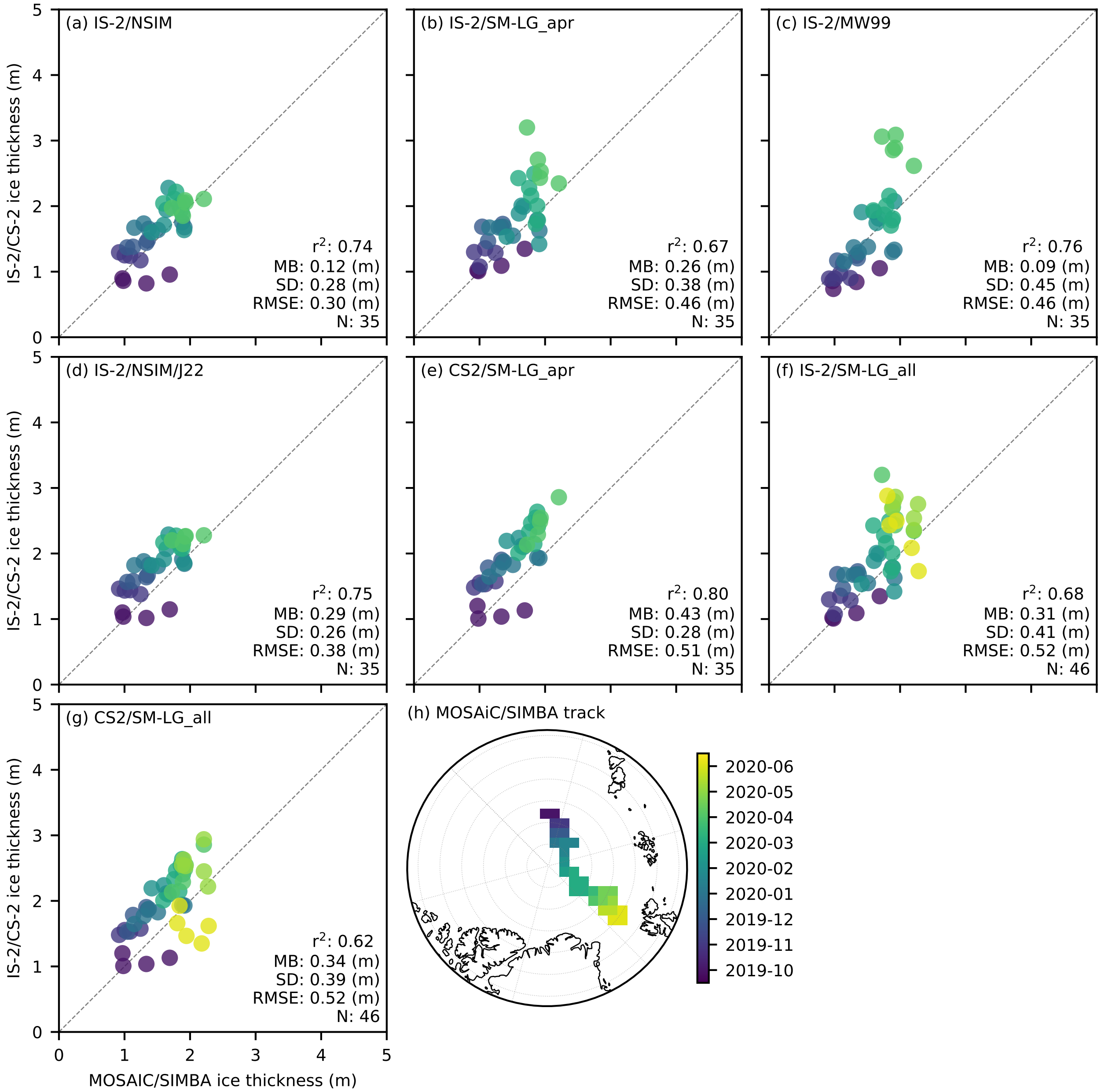


**Fig. 11.** Comparisons of October 2019 to July 2020 MOSAiC/SIMBA buoy ice thickness measurements (binned to a 100 km North Polar Stereographic grid) and coincident monthly mean coarsened ice thickness estimates from ICESat-2 with (a) NESOSIM v1.1 (NSIM) snow loading through to April 2020, (b) SnowModel-LG (SM-LG) snow loading through to April 2020, (c) modified Warren99 snow loading through to April 2020 (MW99), (d) NSIM snow loading and J22 bulk ice density through to April 2020, (e) CryoSat-2/SM-LG data through to April 2020, (f) ICESat-2 and SM-LG snow loading through to June 2020, (g) CryoSat-2/SM-LG data through to June 2020. Panel (h) shows the MOSAiC/SIMBA track color-coded by date, which are used in the colors across all scatter plots.

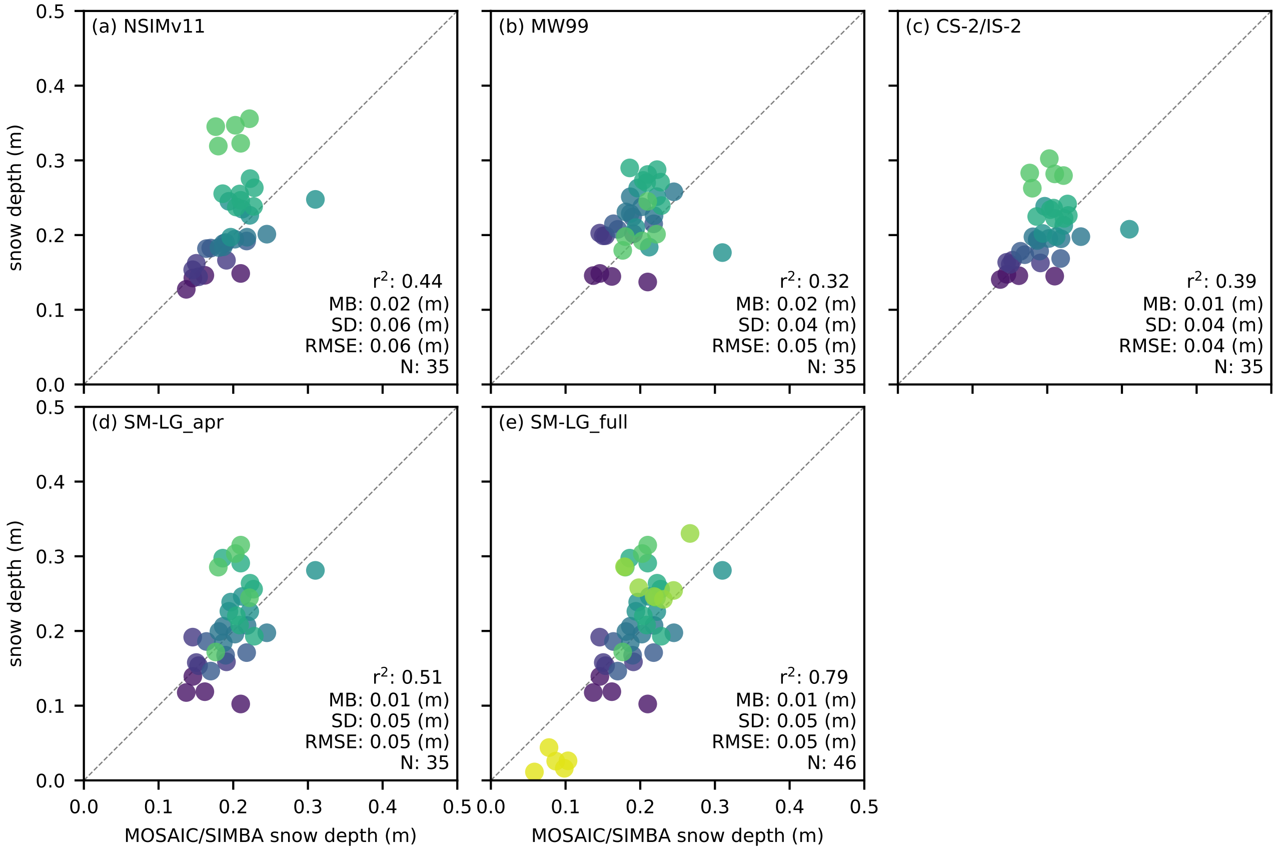


**Fig. 12.** Comparisons of October 2019 to June 2020 MOSAiC/SIMBA buoy snow depth measurements (binned to a 100 km North Polar Stereographic grid) and coincident monthly mean coarsened snow depths (sub-sampled by ICESat-2) from (a) NESOSIM v1.1 snow loading (NSIM) through to April 2020, (b) SnowModel-LG (SM-LG) snow loading through to April 2020, (c) modified Warren 99 snow loading (MW99) through April 2020, (d) SM-LG snow loading through to June 2020. Scatter colors based on the track data shown in Fig. 11.

---

time-period and the full October to June overlapping period. For the October to April comparisons, the four products show broadly similar results, with moderate correlations ($r^2$=0.32, MW99 to 0.51, SM-LG), and very low mean biases (0.01 m to 0.02 m) and RMSEs (0.04 m to 0.06 m). The strong performance of the MW99 climatology is again notable, especially as the MOSAiC/SIMBA buoy track includes more of the Eastern/North Atlantic Arctic sector, further outside the focal region of the station data used to compile the climatology. The IS-2/CS-2 dual altimetry fusion product also performs well, featuring the lowest RMSE of all four products. The NSIM, IS-2/CS-2 and SM-LG products show higher snow depths in April (>30 cm) compared to MOSAiC/SIMBA (∼20 cm), which appears to dominate the reduction in correlation. The representativeness of the MOSAiC/SIMBA buoy data and their utility for characterizing biases is still questionable, which we discuss more later. The earlier time series analysis (Fig. 5) also highlighted the strong consistency between NSIM, MW99 and the IS-2/CS-2 snow depth estimates in the October 2019 to March 2020 period, but with MW99 declining in April 2020 and NSIM/IS-2/CS-2 increasing. Finally, the thinner snow depths in May/June appear well-represented in the SM-LG data (albeit with a slight negative bias), resulting in a significant increase in correlation ($r^2$=0.79) while other metrics remain constant, providing some good, albeit limited, evidence of SM-LG simulating the summer snow depth decline. It is again important to recognize that buoy-derived snow depths are prone to representation issues and are particularly uncertain during the summer melt season.

## 4 DISCUSSION

Our new ICESat-2 all-season thickness estimates perform well overall, showing good agreement with the CryoSat-2/SM-LG all-season product and strong performance across the three independent validation data assessments. Snow depth biases are likely contributing to a significant fraction of the thickness biases observed between our IS-2 and CS-2 thickness estimates. The BGEP ULS comparisons, for example, produced periods of contrasting bias across the IS-2 and CS-2 datasets, which are expected because a snow depth bias will theoretically impact the estimated thickness obtained from CryoSat-2 radar freeboard and ICESat-2 total freeboard observations in opposing directions. For radar and ice freeboard to thickness calculations, the snow depth bias has a strong inverse linear relation to resultant ice thickness bias. For laser and total freeboard to thickness calculations, the impact of a snow depth bias is more complex, as a snow depth bias features in the hydrostatic equilibrium equation in both the freeboard and snow loading component, generally resulting in a thickness bias in an opposite direction, although this depends on the magnitude of the underlying snow density. This is the only variable that results in this contrasting input data bias response. The strong agreement between NESOSIM, MW99 and IS-2/CS-2 altimetry fusion snow depths are suggestive of a potential low bias in the SM-LG snow depths in 2020 and especially 2021. However, quantifying the relative impacts of snow biases is challenging, and it is still possible that the three former products are all biased thick. The use of different bulk ice density estimates between the IS-2 and CS-2 processing also contribute up to 20-30 cm of the 40 cm mean thickness difference between IS-2/SM-LG and CS-2/SM-LG, and while not necessarily producing more accurate absolute results, would help isolate and diagnose remaining sources of bias.

The snow depths from the new preliminary winter Arctic IS-2/CS-2 altimetry fusion dataset (Landy and others, 2024) performed well in our independent validation and showed strong consistency with NESOSIM and MW99 across the three winter periods of overlap. The strong performance of this winter dual altimetry fused snow depth estimate provides further indirect evidence of the reliability of the underlying IS-2 and CS-2 freeboards and the potential to infer snow depth and thickness concurrently (Kacimi and Kwok, 2022; Fredensborg Hansen and others, 2024; Landy and others, 2024; Carret and others, 2025). No clear bias could be detected in the dual-altimetry snow depths that would point to systematic biases in either IS-2 or CS-2 freeboards. A slight thick bias versus the IceBird observations suggests that CS-2 returns are not, at least, scattering from a mean height within the snowpack, although there was only 1 cm bias recorded at the MOSAiC/SIMBAs. It should, in theory, be possible to expand these approaches to summer, leveraging the year-round ICESat-2 freeboards and recent summer CryoSat-2 ice freeboard profiling advances (Dawson and others, 2022).

The MW99 snow climatology still performs surprisingly well, showing the lowest RMSEs in BGEP ULS ice drafts when combined with IS-2 freeboards and high skill in capturing the regional distribution in snow depths observed during IceBird-2019 and MOSAiC/SIMBA (to a lesser degree). The MOSAiC/SIMBA buoys are known to have a low snow thickness bias relative to nearby magnaprobe measurements, possibly as a consequence of the deployment over level ice being more conducive to snow drifting (Lei and others, 2022). Snow conditions in the Central Arctic/Beaufort Sea appear to remain closely linked to variability in ice type (first-year or multiyear ice), which the ice type modified climatology is still principally constrained by. Furthermore, this suggests that large-scale regional and interannual variations in satellite-observed laser or radar freeboard, rather than snow loading, are more important for accurate detection of the same variations in sea ice thickness. The snow accumulation models (NESOSIM v1.1 and SM-LG) and resultant sea ice thicknesses perform well across all validation datasets and better capture the full range in observed snow conditions, but struggle to show consistently more reliable snow depths than MW99 between regions or years. More validation data is needed across different time-periods and especially within the eastern Arctic, where the accumulation models are expected to provide more benefits over MW99 for multiple reasons: (i) these regions provided significantly less input data to MW99, (ii) they have undergone the largest transitions in sea ice and likely snow conditions in recent decades (Stroeve and Notz, 2018; Petty and others, 2018; Cabaj and others, 2024), and (iii) these regions are more susceptible to synoptic-scale snowfall variability, especially in summer (Webster and others, 2019; Lim and others, 2022). Regardless, there is a clear need for further snow model development and calibration efforts.

A notable feature still underexplored in our study is the timing and magnitude of spring/summer snow loss and impacts on thickness. The missing IS-2 in July 2019 prevented a more detailed interannual assessment of this decline, but should form the basis of future work. In May and June the snow still tends to be relatively thick across available datasets, reflecting winter accumulation patterns. SM-LG, however, shows drastic declines in snow depth between June and July across our three-year study period. While mid-late summer snow is generally thin, it can still be highly variable based on synoptic-scale variability (Webster and others, 2019; Lim and others, 2022), and even small differences in snow depth can have a disproportionately large impact on thin ice freeboard and thickness retrievals. July also generally coincides with the period of peak melt pond coverage, depending on region (Niehaus and others, 2024), so issues with miss-classified surfaces in ICESat-2 sea ice data (Tilling and others, 2020) and resultant biases in ice freeboard will also be contributing to anomalous freeboard and thickness reduction and is worth more consideration. The role of potential biases in spring/summer snow melt, melt water load and impacts on CryoSat-2 derived freeboard and thickness estimates was recently discussed in Salganik and others (2025).

In addition, there is an urgent need for expanded year-round validation efforts, particularly a greater number of mooring deployments across the Arctic to complement the limited existing datasets, and especially in the eastern and more peripheral regions of the Arctic. As well as more validation data, we also promote more consideration of spatial and temporal sampling/representativeness to more effectively compare localized validation data against the 25-100 km scales and longer aggregation timescales represented by the satellite products. We also hope to leverage external datasets in future work to better understand surface melt conditions and associated freeboard and thickness retrieval performance in more detail, e.g. isolating periods and regions of maximum/minimum melt pond coverage (Niehaus and others, 2024).

Our focus in this initial all-season assessment was on monthly to inter-annual thickness skill, but future work could explore daily to weekly skill, which should again include deeper consideration of optimal spatial and temporal sampling of the variable IS-2/CS-2 orbit cycles. Orbit aliasing was still present in our interpolated/smoothed IS-2 June gridded thickness estimates, motivating the need for improved interpolation routines. Along-track IS-2 thickness data are available (Petty and others, 2022) that can enable more direct comparisons with CS-2 and reducing gridding/resampling error, especially leveraging the increased orbit alignments generated through the Cryo2Ice initiative (Fredensborg Hansen and others, 2024). In addition, more sophisticated altimetry interpolation routines have been proposed that could be better leveraged to enhance grid-cell representativeness across scales (Gregory and others, 2021).

## 5 CONCLUSION

We have presented an initial analysis of all-season ICESat-2 Arctic sea ice thickness by combining ICESat-2 freeboards with all-season SnowModel-LG snow loading. Our assessments show that the ICESat-2 thickness retrievals capture key regional and seasonal patterns of Arctic sea ice variability and agree well with recently published CryoSat-2 all-season estimates. Regional differences remain, with IS-2 generally showing thicker ice north of Greenland and the Canadian Arctic Archipelago, which was highlighted in the original development studies (Dawson and others, 2022; Landy and others, 2022) as an uncertain region for CryoSat-2 summer observations. However, these summer differences are largely consistent with the winter differences, suggesting only secondary impacts of summer conditions impacting the biases between the two products. Validation against three different independent datasets, including BGEP ULS moorings, IceBird-2019 airborne surveys, and MOSAiC/SIMBA buoy observations, highlights generally good skill across a range of ice conditions, although some regional and seasonal biases remain.

The choice of snow model inputs and ice density assumptions continues to have a strong influence on absolute thickness estimates. Differences between ICESat-2 and CryoSat-2 thicknesses are consistent with expected sensitivities to snow depth biases, freeboard retrieval differences, and the underlying treatment of multi-year versus first-year ice and resultant density estimates. Some additional concerns relating to the timing and magnitude of the spring/summer snow depth decline and expected impact on thickness decline require further investigation.

While our results are encouraging, they also emphasize the need for further work to better constrain summer snow conditions, refine the freeboard-to-thickness input assumptions, and expand independent evaluation datasets and analysis across Arctic regions and time-periods. Continued development of snow accumulation models, new density parameterizations, and data fusion approaches will be key to improving all-season Arctic sea ice thickness retrievals. Importantly, if satellite-derived thickness estimates are to enhance or benchmark state-of-the-art seasonal-to-climate prediction systems, they need to accurately capture inter-annual variability at regional scales of interest. While our results are promising, a longer record and further evaluation against independent observations are needed to better characterize and reduce potential biases through the freeboard-to-thickness processing chain.

## 6 ACKNOWLEDGMENTS

AP was supported by NASA's ICESat-2 Science Team award: 80NSSC23K1253 and NASA's Cryospheric Sciences award: 80NSSC23K1253. JL was partially supported by the Research Council of Norway projects INTERAAC: 328957 and DynAMIC: 343069, the European Research Council project SI/3D: 101077496, and the SUDARCO (Forskning for god forvaltning av Polhavet) project under the Fram Centre: 2551323. We would like to thank all members of the NASA ICESat-2 and ESA CryoSat-2 teams for their continued efforts in developing and maintaining these missions and associated sea ice datasets. We would also like to thank the the BGEP, IceBird and MOSAiC teams for their considerable efforts in collecting and sharing the crucial evaluation datasets.

## 7 SUPPLEMENTARY MATERIAL

Supplementary Material for this paper can be found at [provide link on publication]

## REFERENCES

Blair J, Hofton M, Kurtz N and Harbeck J (2023) ICESat-2 Calibration/Validation LVIS L1B Georeferenced Imagery, Version 1 (doi: 10.5067/K1EYYP0SL2PF)

Cabaj A, Kushner PJ and Petty AA (2024) Investigating the impact of reanalysis snow input on an observationally calibrated snow-on-sea-ice reconstruction. *EGUsphere*, 1–37 (doi: 10.5194/egusphere-2024-2562)

Carret A, Fleury S, Di Bella A, Landy J, Lawrence I, Kurtz N, Laforge A, Bouffard J and Parrinello T (2025) A multi-frequency altimetry snow depth product over Arctic sea ice. *Scientific Data*, **12**(1), 104, ISSN 2052-4463 (doi: 10.1038/s41597-024-04343-4)

Cohen J, Screen JA, Furtado JC, Barlow M, Whittleston D, Coumou D, Francis J, Dethloff K, Entekhabi D, Overland J and Jones J (2014) Recent Arctic amplification and extreme mid-latitude weather. *Nature Geosci*, **7**(9), 627–637, ISSN 1752-0894

Dawson G, Landy J, Tsamados M, Komarov AS, Howell S, Heorton H and Krumpen T (2022) A 10-year record of Arctic summer sea ice freeboard from CryoSat-2. *Remote Sensing of Environment*, **268**, 112744, ISSN 0034-4257 (doi: 10.1016/j.rse.2021.112744)

Fredensborg Hansen RM, Skourup H, Rinne E, Høyland KV, Landy JC, Merkouriadi I and Forsberg R (2024) Arctic Freeboard and Snow Depth From Near-Coincident CryoSat-2 and ICESat-2 (CRYO2ICE) Observations: A

First Examination of Winter Sea Ice During 2020–2022. *Earth and Space Science*, **11**(4), e2023EA003313, ISSN 2333-5084 (doi: 10.1029/2023EA003313)

Gregory W, Lawrence IR and Tsamados M (2021) A Bayesian approach towards daily pan-Arctic sea ice freeboard estimates from combined CryoSat-2 and Sentinel-3 satellite observations. *The Cryosphere*, **15**(6), 2857–2871, ISSN 1994-0416 (doi: 10.5194/tc-15-2857-2021)

Haas C, Beckers J, King J, Silis A, Stroeve J, Wilkinson J, Notenboom B, Schweiger A and Hendricks S (2017) Ice and Snow Thickness Variability and Change in the High Arctic Ocean Observed by In Situ Measurements. *Geophysical Research Letters*, **44**(20), 10,462–10,469, ISSN 1944-8007 (doi: 10.1002/2017GL075434)

Jutila A, Hendricks S, Ricker R, von Albedyll L, Krumpen T and Haas C (2022) Retrieval and parameterisation of sea-ice bulk density from airborne multi-sensor measurements. *The Cryosphere*, **16**(1), 259–275, ISSN 1994-0416 (doi: 10.5194/tc-16-259-2022)

Jutila A, Hendricks S, Ricker R, von Albedyll L and Haas C (2024) Airborne sea ice parameters during aircraft flight P6_217_icebird_2019_1904051001, Version 2 (doi: 10.1594/PANGAEA.966059), publication Title: In: Jutila, A et al. (2024): Airborne sea ice parameters during the IceBird Winter 2019 campaign in the Arctic Ocean, Version 2 [dataset publication series]. PANGAEA, https://doi.org/10.1594/PANGAEA.966057

Kacimi S and Kwok R (2022) Arctic Snow Depth, Ice Thickness, and Volume From ICESat-2 and CryoSat-2: 2018–2021. *Geophysical Research Letters*, **49**(5), e2021GL097448, ISSN 1944-8007 (doi: 10.1029/2021GL097448)

Krishfield RA, Proshutinsky A, Tateyama K, Williams WJ, Carmack EC, McLaughlin FA and Timmermans ML (2014) Deterioration of perennial sea ice in the Beaufort Gyre from 2003 to 2012 and its impact on the oceanic freshwater cycle. *J. Geophys. Res. Oceans*, **119**(2), 1271–1305, ISSN 2169-9291 (doi: 10.1002/2013JC008999)

Kwok R (2018) Arctic sea ice thickness, volume, and multiyear ice coverage: losses and coupled variability (1958–2018). *Environmental Research Letters*, **13**(10), 105005, ISSN 1748-9326 (doi: 10.1088/1748-9326/aae3ec)

Kwok R and Cunningham GF (2008) ICESat over Arctic sea ice: Estimation of snow depth and ice thickness. *Journal of Geophysical Research: Oceans*, **113**(C8), C08010, ISSN 2156-2202 (doi: 10.1029/2008JC004753)

Kwok R, Kacimi S, Markus T, Kurtz NT, Studinger M, Sonntag JG, Manizade SS, Boisvert LN and Harbeck JP (2019a) ICESat-2 surface height and sea-ice freeboard assessed with ATM lidar acquisitions from Operation IceBridge. *Geophysical Research Letters*, **44**, 11228– 11236, ISSN 1944-8007 (doi: 10.1029/2019GL084976)

Kwok R, Markus T, Kurtz NT, Petty AA, Neumann TA, Farrell SL, Cunningham GF, Hancock DW, Ivanoff A and Wimert JT (2019b) Surface Height and Sea Ice Freeboard of the Arctic Ocean From ICESat-2: Characteristics and Early Results. *Journal of Geophysical Research: Oceans*, **124**(10), 6942–6959, ISSN 2169-9291 (doi: 10.1029/2019JC015486)

Kwok R, Kacimi S, Webster MA, Kurtz NT and Petty AA (2020) Arctic Snow Depth and Sea Ice Thickness From ICESat-2 and CryoSat-2 Freeboards: A First Examination. *Journal of Geophysical Research: Oceans*, **125**(3), e2019JC016008, ISSN 2169-9291 (doi: 10.1029/2019JC016008)

Kwok R, Petty AA, Bagnardi M, Kurtz NT, Cunningham GF, Ivanoff A and Kacimi S (2021) Refining the sea surface identification approach for determining freeboards in the ICESat-2 sea ice products. *The Cryosphere*, **15**(2), 821–833, ISSN 1994-0416 (doi: 10.5194/tc-15-821-2021)

Landy JC, Dawson GJ, Tsamados M, Bushuk M, Stroeve JC, Howell SEL, Krumpen T, Babb DG, Komarov AS, Heorton HDBS, Belter HJ and Aksenov Y (2022) A year-round satellite sea-ice thickness record from CryoSat-2. *Nature*, **609**(7927), 517–522, ISSN 1476-4687 (doi: 10.1038/s41586-022-05058-5)

Landy JC, de Rijke-Thomas C, Nab C, Lawrence I, Glissenaar IA, Mallett RDC, Fredensborg Hansen RM, Petty A, Tsamados M, Macfarlane AR and Braakmann-Folgmann A (2024) Anticipating CRISTAL: An exploration of multi-frequency satellite altimeter snow depth estimates over Arctic sea ice, 2018–2023. *EGUsphere*, 1–41 (doi: 10.5194/egusphere-2024-2904)

Lei R, Cheng B, Hoppmann M, Zhang F, Zuo G, Hutchings JK, Lin L, Lan M, Wang H, Regnery J, Krumpen T, Haapala J, Rabe B, Perovich DK and Nicolaus M (2022) Seasonality and timing of sea ice mass balance and heat fluxes in the Arctic transpolar drift during 2019–2020. *Elementa: Science of the Anthropocene*, **10**(1), 000089, ISSN 2325-1026 (doi: 10.1525/elementa.2021.000089)

Lim WI, Park HS, Petty AA and Seo KH (2022) The Role of Summer Snowstorms on Seasonal Arctic Sea Ice Loss. *Journal of Geophysical Research: Oceans*, **127**(12), e2021JC018066, ISSN 2169-9291 (doi: 10.1029/2021JC018066)

Liston GE, Itkin P, Stroeve J, Tschudi M, Stewart JS, Pedersen SH, Reinking AK and Elder K (2020) A Lagrangian Snow-Evolution System for Sea-Ice Applications (SnowModel-LG): Part I—Model Description. *Journal of Geophysical Research: Oceans*, **125**(10), e2019JC015913, ISSN 2169-9291 (doi: 10.1029/2019JC015913)

Markus T, Neumann T, Martino A, Abdalati W, Brunt K, Csatho B, Farrell S, Fricker H, Gardner A, Harding D, Jasinski M, Kwok R, Magruder L, Lubin D, Luthcke S, Morison J, Nelson R, Neuenschwander A, Palm S, Popescu S, Shum C, Schutz BE, Smith B, Yang Y and Zwally J (2017) The Ice, Cloud, and land Elevation Satellite-2 (ICESat-2): Science requirements, concept, and implementation. *Remote Sensing of Environment*, **190**, 260–273, ISSN 0034-4257 (doi: 10.1016/j.rse.2016.12.029)

Massonnet F, Vancoppenolle M, Goosse H, Docquier D, Fichefet T and Blanchard-Wrigglesworth E (2018) Arctic sea-ice change tied to its mean state through thermodynamic processes. *Nature Climate Change*, **8**(7), 599, ISSN 1758-6798 (doi: 10.1038/s41558-018-0204-z)

Meier WN, Hovelsrud GK, van Oort BE, Key JR, Kovacs KM, Michel C, Haas C, Granskog MA, Gerland S, Perovich DK, Makshtas A and Reist JD (2014) Arctic sea ice in transformation: A review of recent observed changes and impacts on biology and human activity. *Reviews of Geophysics*, **52**(3), 2013RG000431, ISSN 1944-9208 (doi: 10.1002/2013RG000431)

Meier WN, Fetterer F, Windnagel AK and Stewart JS (2021) NOAA/NSIDC Climate Data Record of Passive Microwave Sea Ice Concentration, Version 4. *Boulder, Colorado USA. NSIDC: National Snow and Ice Data Center* (doi: 10.7265/efmz-2t65)

Nab C, Mallett R, Nelson C, Stroeve J and Tsamados M (2024) Optimising Interannual Sea Ice Thickness Variability Retrieved From CryoSat-2. *Geophysical Research Letters*, **51**(21), e2024GL111071, ISSN 1944-8007 (doi: 10.1029/2024GL111071)

Nicolaus M, Perovich DK, Spreen G, Granskog MA, von Albedyll L, Angelopoulos M, Anhaus P, Arndt S, Belter HJ, Bessonov V, Birnbaum G, Brauchle J, Calmer R, Cardellach E, Cheng B, Clemens-Sewall D, Dadic R, Damm E, de Boer G, Demir O, Dethloff K, Divine DV, Fong AA, Fons S, Frey MM, Fuchs N, Gabarró C, Gerland S, Goessling HF, Gradinger R, Haapala J, Haas C, Hamilton J, Hannula HR, Hendricks S, Herber A, Heuzé C, Hoppmann M, Høyland KV, Huntemann M, Hutchings JK, Hwang B, Itkin P, Jacobi HW, Jaggi M, Jutila A, Kaleschke L, Katlein C, Kolabutin N, Krampe D, Kristensen SS, Krumpen T, Kurtz N, Lampert A, Lange BA, Lei R, Light B, Linhardt F, Liston GE, Loose B, Macfarlane AR, Mahmud M, Matero IO, Maus S, Morgenstern A, Naderpour R, Nandan V, Niubom A, Oggier M, Oppelt N, Pätzold F, Perron C, Petrovsky T, Pirazzini R, Polashenski C, Rabe B, Raphael IA, Regnery J, Rex M, Ricker R, Riemann-Campe K, Rinke A, Rohde J, Salganik E, Scharien RK, Schiller M, Schneebeli M, Semmling M, Shimanchuk E, Shupe MD, Smith MM, Smolyanitsky V, Sokolov V, Stanton T, Stroeve J, Thielke L, Timofeeva A, Tonboe RT, Tavri A, Tsamados M, Wagner DN, Watkins D, Webster M and Wendisch M (2022) Overview of the MOSAiC expedition: Snow and sea ice. *Elementa: Science of the Anthropocene*, **10**(1), 000046, ISSN 2325-1026 (doi: 10.1525/elementa.2021.000046)

Niehaus H, Spreen G, Istomina L and Nicolaus M (2024) Regional and seasonal evolution of melt ponds on Arctic sea ice. *EGUsphere*, 1–36 (doi: 10.5194/egusphere-2024-3127)

Notz D and Stroeve J (2016) Observed Arctic sea-ice loss directly follows anthropogenic CO2 emission. *Science*, **354**(6313), 747–750, ISSN 0036-8075, 1095-9203 (doi: 10.1126/science.aag2345)

Petty A, Kwok R, Bagnardi M, Ivanoff A, Kurtz D, Lee J and Wimert J (2023a) ATLAS/ICESat-2 L3B Daily and

Monthly Gridded Sea Ice Freeboards, Version 4. *Boulder, Colorado USA. NSIDC: National Snow and Ice Data Center* (doi: 10.5067/ATLAS/ATL20.004)

Petty AA, Webster M, Boisvert L and Markus T (2018) The NASA Eulerian Snow on Sea Ice Model (NESOSIM) v1.0: initial model development and analysis. *Geoscientific Model Development*, **11**(11), 4577–4602, ISSN 1991-959X (doi: https://doi.org/10.5194/gmd-11-4577-2018)

Petty AA, Kurtz NT, Kwok R, Markus T and Neumann TA (2020) Winter Arctic Sea Ice Thickness From ICESat-2 Freeboards. *Journal of Geophysical Research: Oceans*, **125**(5), e2019JC015764, ISSN 2169-9291 (doi: 10.1029/2019JC015764)

Petty AA, Kurtz N, Kwok R, Markus T and Neumann TA (2022) ICESat-2 L4 Along-Track Sea Ice Thickness, Version 1. *Boulder, Colorado USA. NASA National Snow and Ice Data Center Distributed Active Archive Center* (doi: 10.5067/JTI5YG3S6VAJ)

Petty AA, Keeney N, Cabaj A, Kushner P and Bagnardi M (2023b) Winter Arctic sea ice thickness from ICESat-2: upgrades to freeboard and snow loading estimates and an assessment of the first three winters of data collection. *The Cryosphere*, **17**(1), 127–156, ISSN 1994-0416 (doi: 10.5194/tc-17-127-2023)

Petty AA, Kurtz N, Kwok R, Markus T, Neumann TA and Keeney N (2023c) ICESat-2 L4 Monthly Gridded Sea Ice Thickness, Version 3. *Boulder, Colorado USA. NASA National Snow and Ice Data Center Distributed Active Archive Center* (doi: 10.5067/ZCSU8Y5U1BQW)

Polyakov IV, Ingvaldsen RB, Pnyushkov AV, Bhatt US, Francis JA, Janout M, Kwok R and Skagseth O (2023) Fluctuating Atlantic inflows modulate Arctic atlantification. *Science*, **381**(6661), 972–979 (doi: 10.1126/science.adh5158)

Post E, Bhatt US, Bitz CM, Brodie JF, Fulton TL, Hebblewhite M, Kerby J, Kutz SJ, Stirling I and Walker DA (2013) Ecological Consequences of Sea-Ice Decline. *Science*, **341**(6145), 519–524, ISSN 0036-8075, 1095-9203 (doi: 10.1126/science.1235225)

Ricker R, Hendricks S, Kaleschke L, Tian-Kunze X, King J and Haas C (2017) A weekly Arctic sea-ice thickness data record from merged CryoSat-2 and SMOS satellite data. *The Cryosphere*, **11**(4), 1607–1623, ISSN 1994-0416 (doi: https://doi.org/10.5194/tc-11-1607-2017)

Salganik E, Crabeck O, Fuchs N, Hutter N, Anhaus P and Landy JC (2025) Impacts of air fraction increase on Arctic sea ice density, freeboard, and thickness estimation during the melt season. *The Cryosphere*, **19**(3), 1259–1278, ISSN 1994-0416 (doi: 10.5194/tc-19-1259-2025)

Saylam DK, Averett AR, Andrews JR, Short SR, Kurtz NT and Tilling RL (2025) Airborne lidar to verify ICESat-2 Arctic summer sea ice heights and melt pond bathymetry: Calibration and validation campaign, Greenland 2022

Song R, Mu L, Loza SN, Kauker F and Chen X (2024) Assimilating Summer Sea-Ice Thickness Observations Improves Arctic Sea-Ice Forecast. *Geophysical Research Letters*, **51**(13), e2024GL110405, ISSN 1944-8007 (doi: 10.1029/2024GL110405)

Stroeve J and Notz D (2018) Changing state of Arctic sea ice across all seasons. *Environmental Research Letters*, **13**(10), 103001, ISSN 1748-9326 (doi: 10.1088/1748-9326/aade56)

Tilling R, Kurtz NT, Bagnardi M, Petty AA and Kwok R (2020) Detection of Melt Ponds on Arctic Summer Sea Ice From ICESat-2. *Geophysical Research Letters*, **47**(23), e2020GL090644, ISSN 1944-8007 (doi: 10.1029/2020GL090644)

Tilling RL, Ridout A and Shepherd A (2018) Estimating Arctic sea ice thickness and volume using CryoSat-2 radar altimeter data. *Advances in Space Research*, **62**(6), 1203–1225, ISSN 0273-1177 (doi: 10.1016/j.asr.2017.10.051)

Warren SG, Rigor IG, Untersteiner N, Radionov VF, Bryazgin NN, Aleksandrov YI and Colony R (1999) Snow Depth on Arctic Sea Ice. *Journal of Climate*, **12**(6), 1814–1829, ISSN 0894-8755 (doi: 10.1175/1520-0442(1999)012<1814:SDOASI>2.0.CO;2)

Webster MA, Parker C, Boisvert L and Kwok R (2019) The role of cyclone activity in snow accumulation on Arctic sea ice. *Nature Communications*, **10**(1), 5285, ISSN 2041-1723 (doi: 10.1038/s41467-019-13299-8)

# Supplementary Material for "Initial assessment of all-season Arctic sea ice thickness from ICESat-2"

Alek PETTY[1], Alex CABAJ[2], Jack LANDY[3]

[1]*Earth System Science Interdisciplinary Center, University of Maryland, MD, USA*

[2]*Environment and Climate Change, Toronto, Canada*

[3]*UiT The Arctic University of Norway, Tromsø, Norway*

*Correspondence: Alek Petty <akpetty@umd.edu>*

## CONTENTS

22 # FIGURES

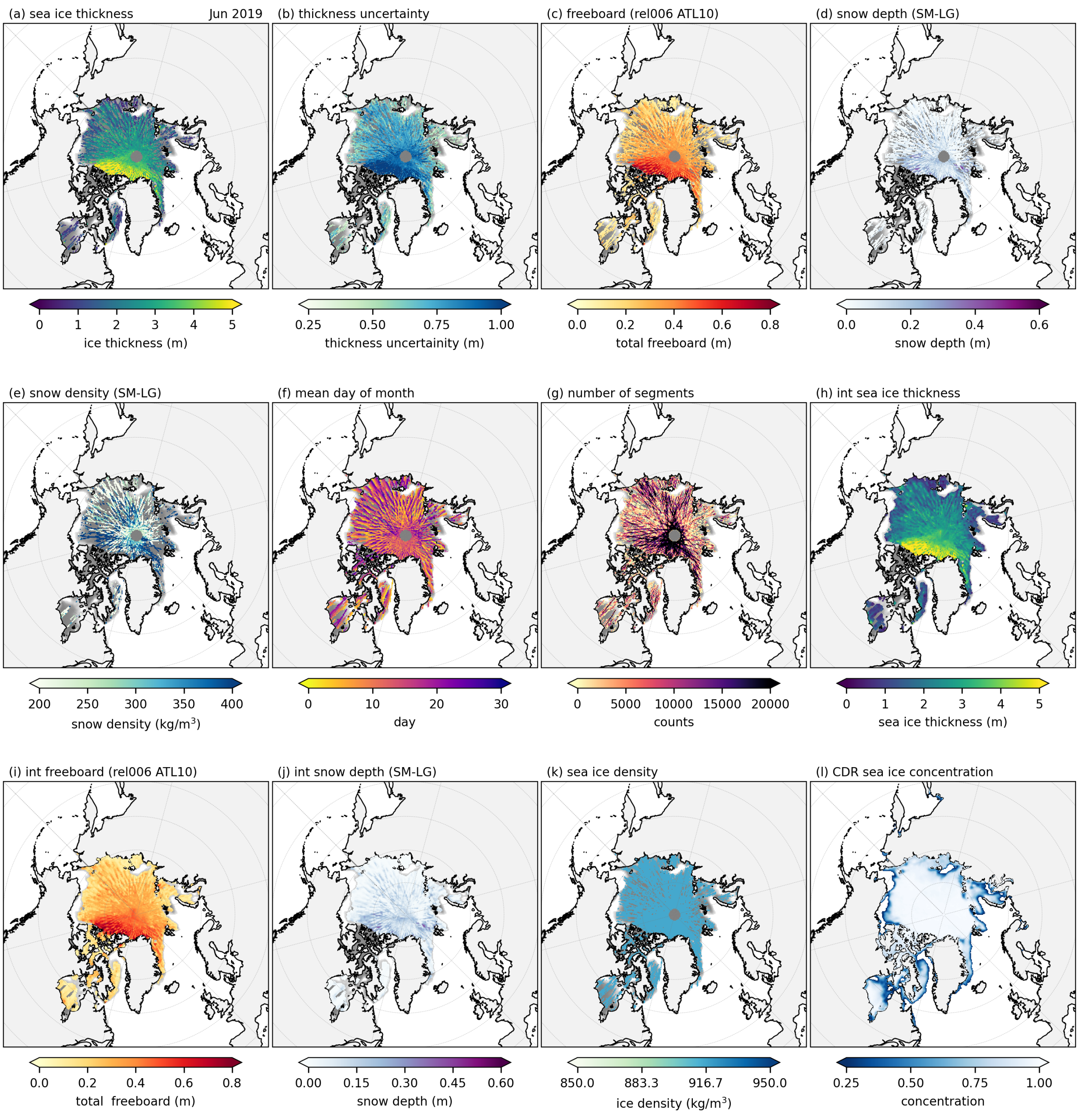


**Fig. S1.** IS2SITMOGR4S browse image for June 2019.

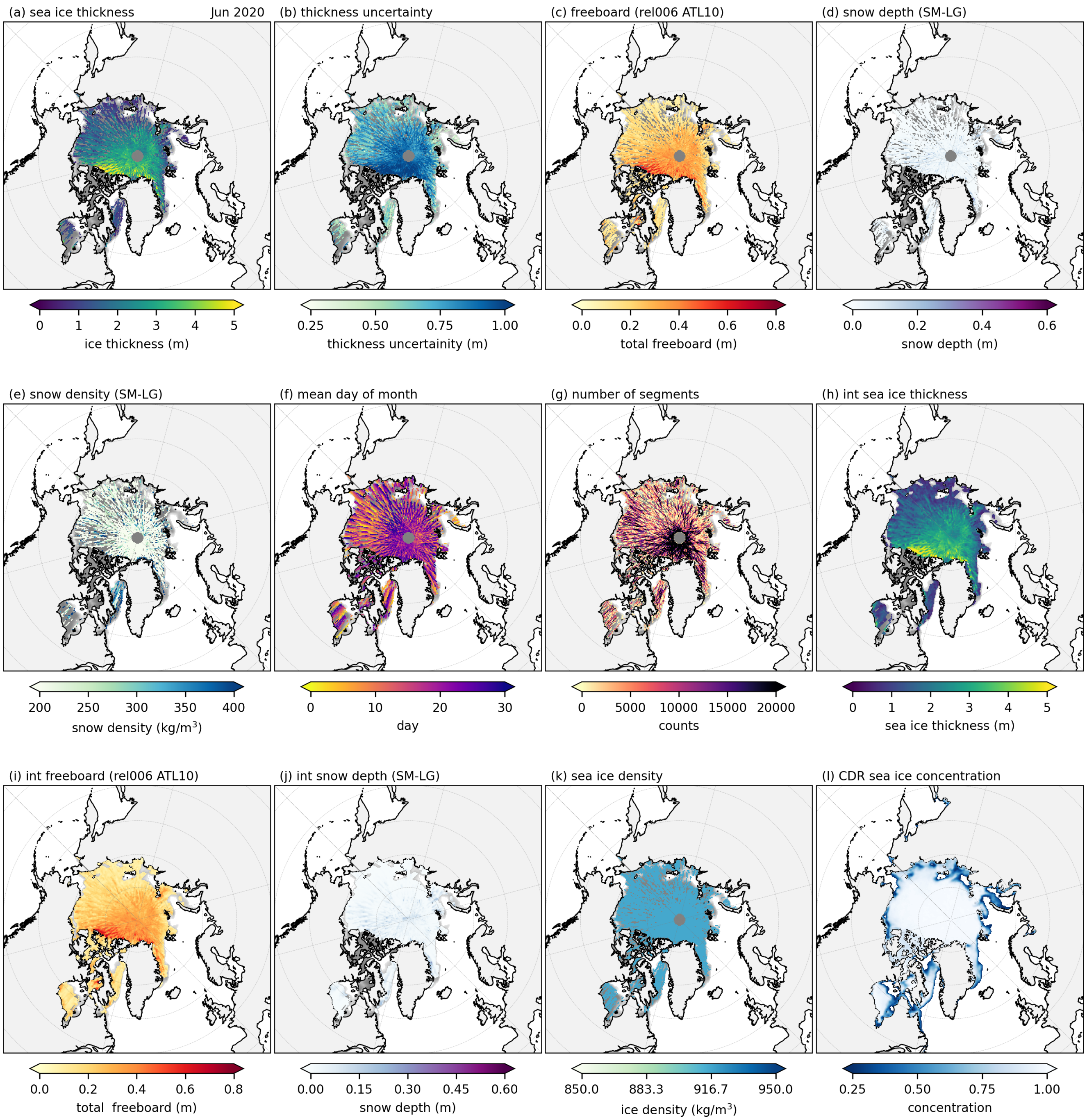


**Fig. S2.** IS2SITMOGR4S browse image for June 2020.

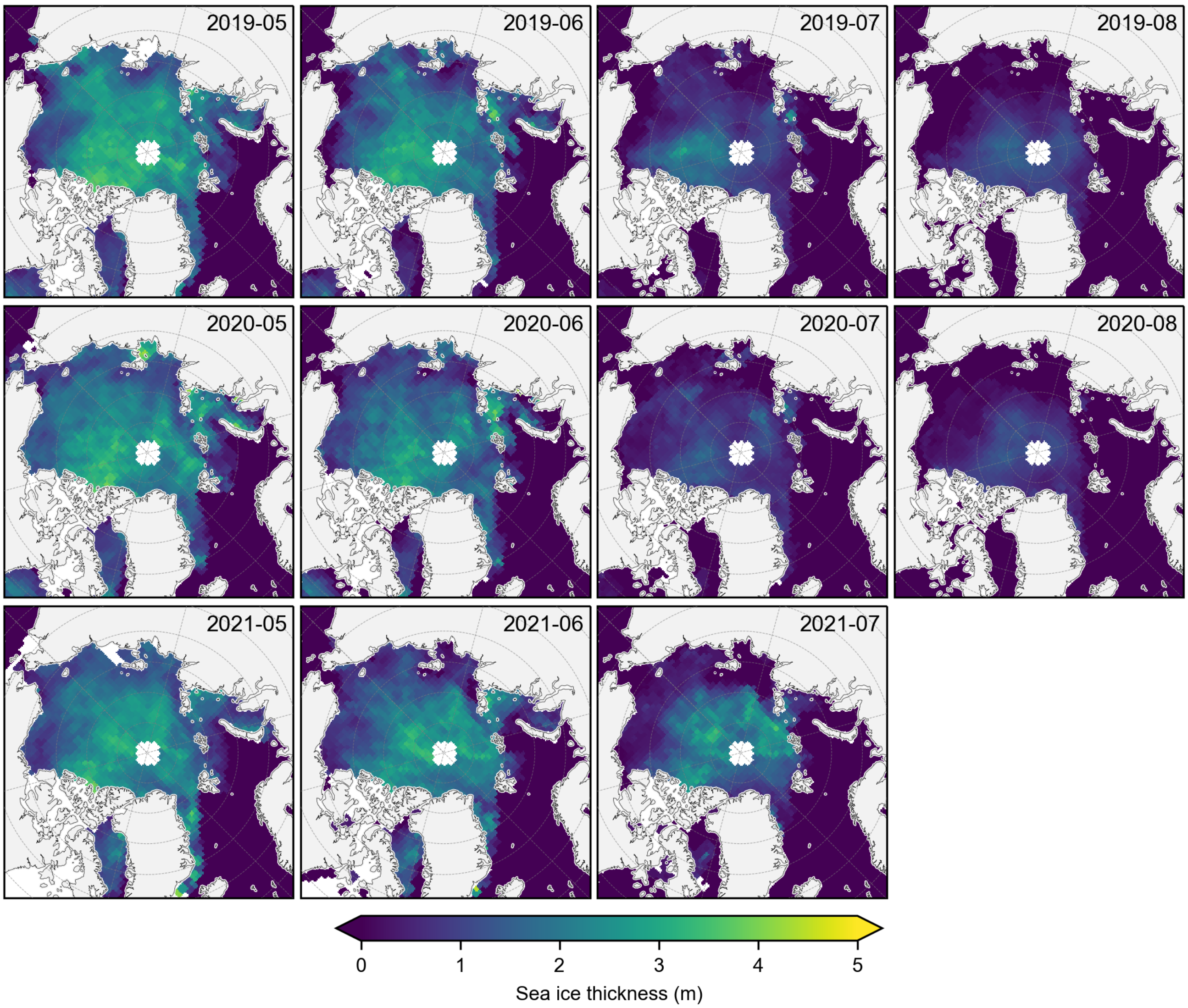


**Fig. S3.** Monthly mean summer (May through August, 2019 to 2021) Arctic sea ice thickness estimates from the UBRIS CryoSat-2/SnowModel-LG all-season thickness dataset.

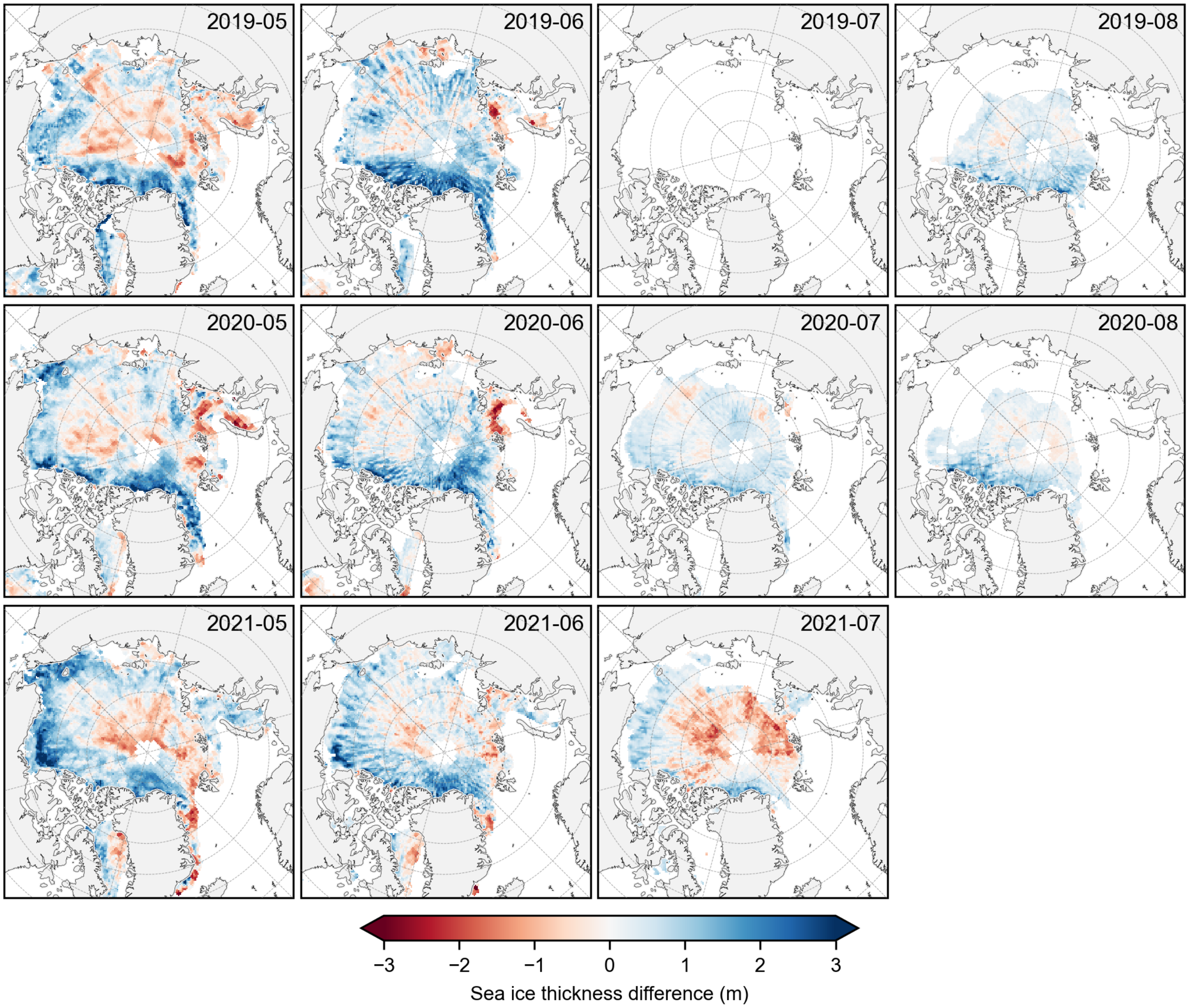


**Fig. S4.** Monthly mean summer (May through August, 2019 to 2021) Arctic sea ice thickness differences between ICESat-2/SnowModel-LG (IS2SITMOGR4S) and CryoSat-2/SnowModel-LG data (UBRIS).

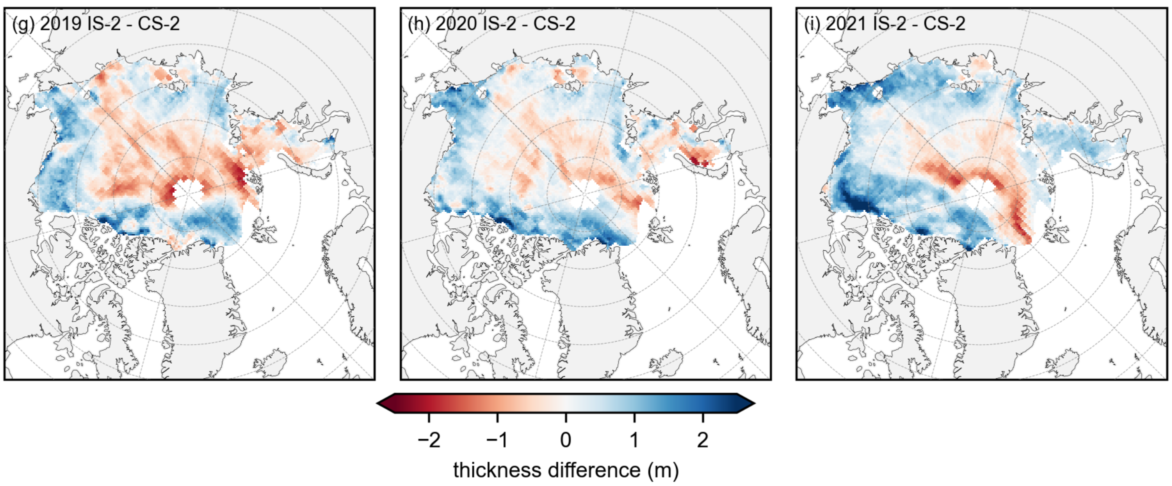


**Fig. S5.** Winter mean (January through April) monthly gridded sea ice thickness difference between ICESat-2/SnowModel-LG (IS-2) and CryoSat-2/SnowModel-LG data (CS-2) for 2019 (a) 2019, (b) 2020 and (c) 2021. The monthly data are filtered where both datasets show consistent monthly data across both datasets (a perennial common mask) before averaging.

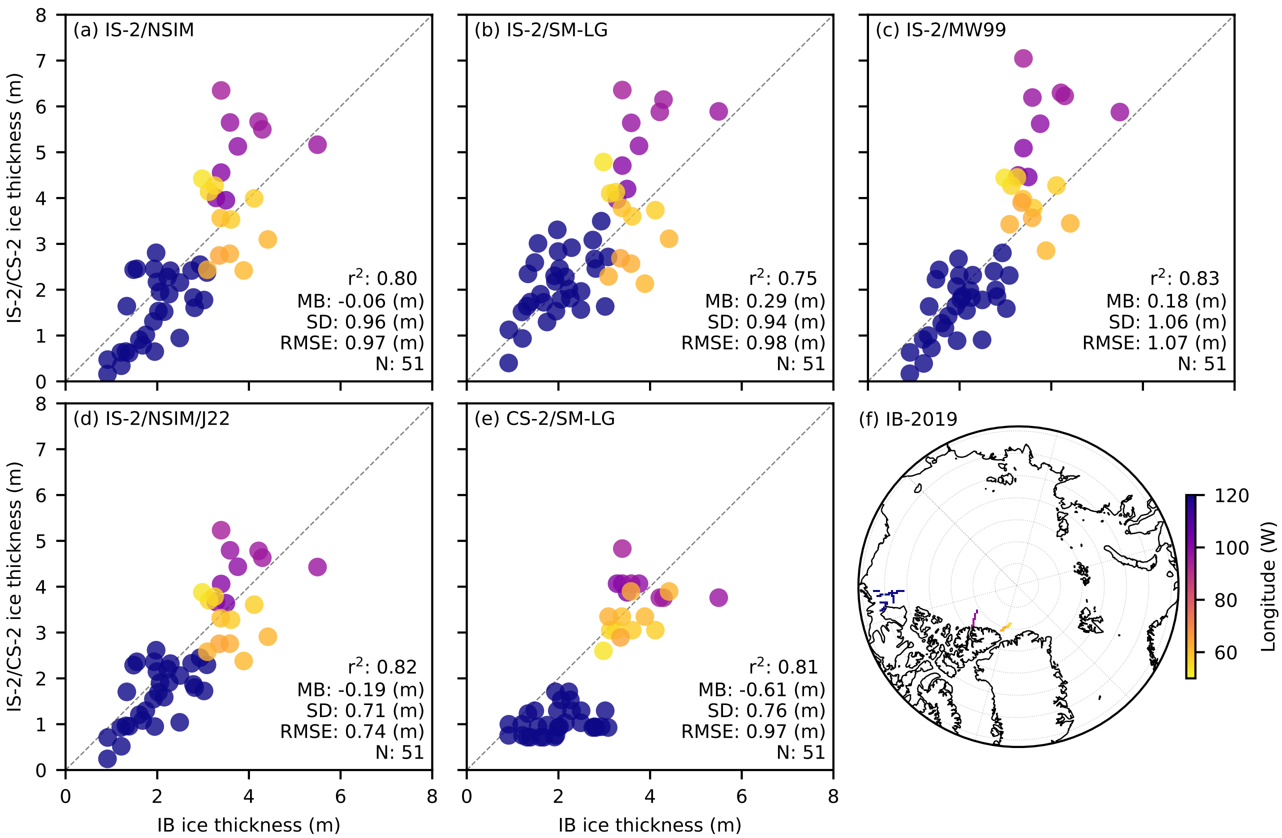


**Fig. S6.** Comparison of AWI IceBird ice thickness observations in April 2019 (binned to a 25 km North Polar Stereographic grid) and coincident monthly mean 100 km coarsened ice thickness from ICESat-2 with four different input assumptions (a) NESOSIM v1.1 snow loading as in IS2SITMOGR4 (b) SM-LG snow loading, (d) mW99 snow loading, (e) J22 ice density and also (f) winter CryoSat-2/SM-LG data. Panel (c) shows the IceBird 2019 flight-lines color-coded by longitude, which are used in the colors across all scatter plots.

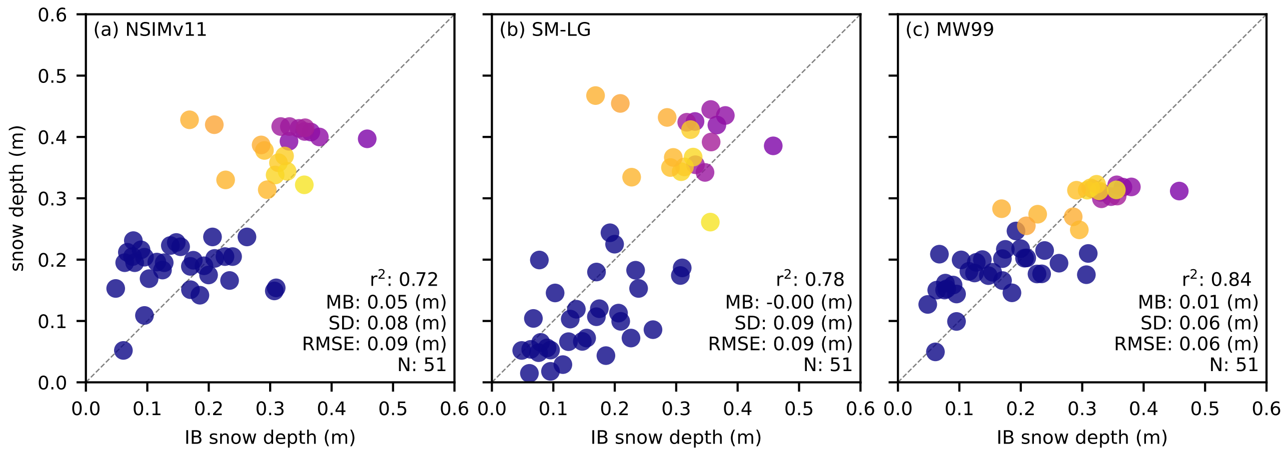


**Fig. S7.** Comparison of AWI IceBird snow depth observations in April 2019 (binned to a 25 km North Polar Stereographic grid) and coincident monthly mean coarsened snow depths (sub-sampled by ICESat-2) from (a) NESOSIM v1.1 snow loading (NSIM) as in IS2SITMOGR4 (b) SM-LG snow loading (SM-LG), and (c) modified Warren 99 (MW99) snow loading. Scatter colors are based on the locations shown in Fig. S6.

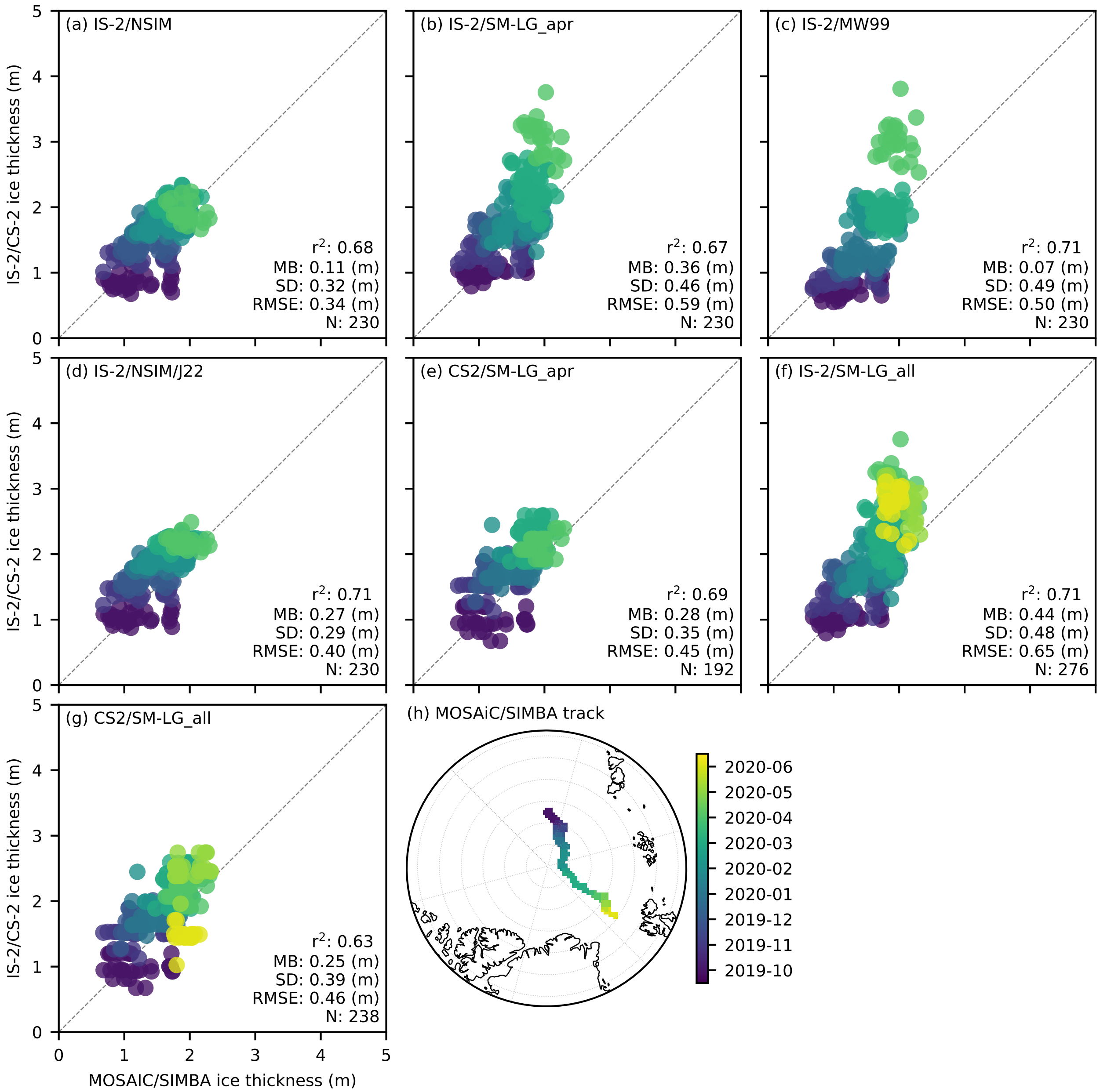


**Fig. S8.** Comparisons of October 2019 to June 2020 MOSAiC/SIMBA buoy ice thickness measurements (binned to a 25 km North Polar Stereographic grid) and coincident monthly mean coarsened ice thickness estimates from ICESat-2 with (a) NESOSIM v1.1 snow loading as in IS2SITMOGR4 through to April 2020, (b) SnowModel-LG snow loading through to April 2020, (c) MW99 snow loading through April 2020, (d) J22 ice density through April 2020, (e) CryoSat-2 and SM-LG data through to April 2020, (f) ICESat-2 and SM-LG snow loading through to June 2020, (g) CryoSat-2 and SM-LG data through to June 2020. Panel (h) shows the MOSAiC/SIMBA track color-coded by date, which are used in the colors across all scatter plots.

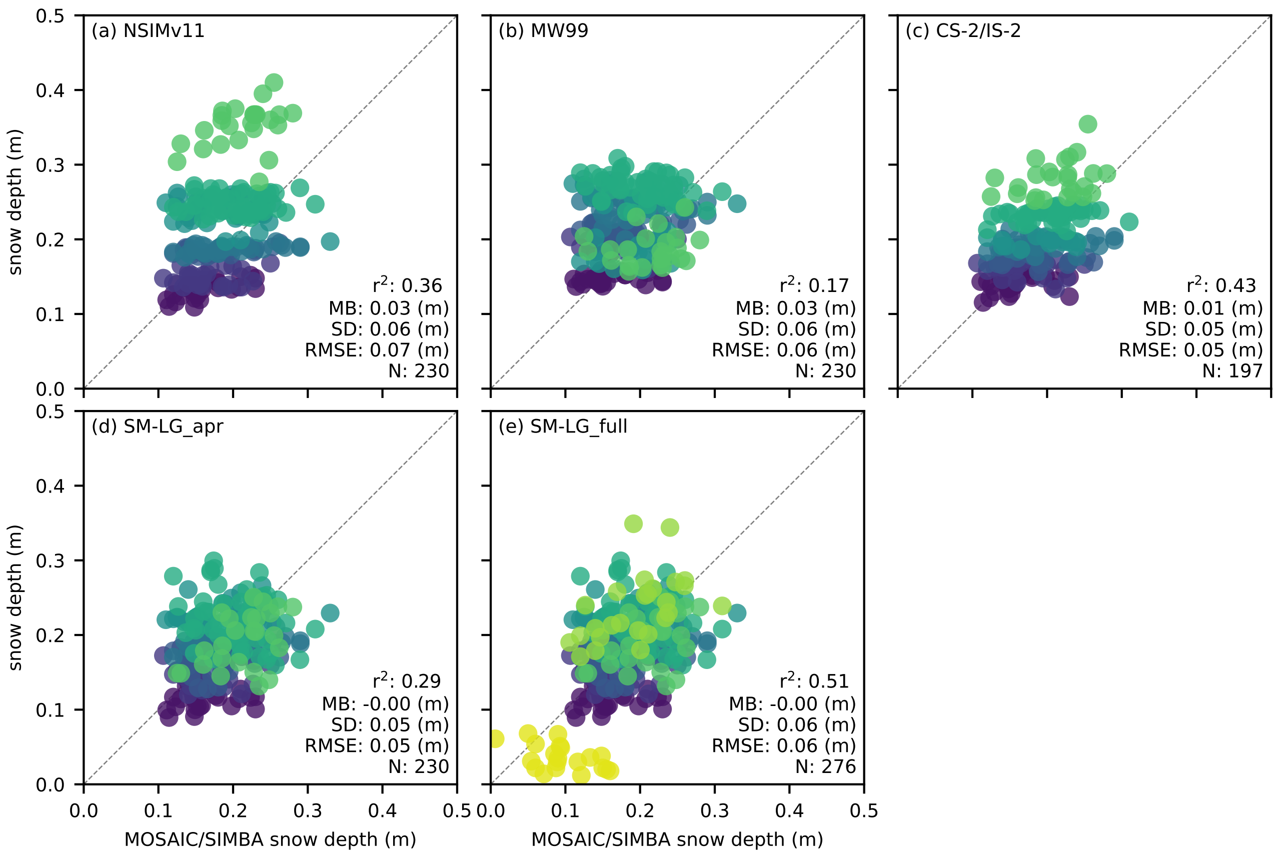


**Fig. S9.** Comparisons of October 2019 to June 2020 MOSAiC/SIMBA buoy snow depth measurements (binned to a 25 km North Polar Stereographic grid) and coincident monthly mean coarsened snow depths (sub-sampled by ICESat-2) from (a) NESOSIM v1.1 snow loading as in IS2SITMOGR4 through to April 2020, (b) SnowModel-LG snow loading through to April 2020, (c) MW99 snow loading through April 2020, (d) SnowModel-LG snow loading through to June 2020. Scatter colors based on the track dates shown in Fig. S8.